nature human behaviour

ARTICLES

https://doi.org/10.1038/s41562-019-0767-3

Deforming the metric of cognitive maps distorts memory

Jacob L. S. Bellmund[1,2,3*], William de Cothi[4,5], Tom A. Ruiter[2,6], Matthias Nau[1,2], Caswell Barry[5,7] and Christian F. Doeller[1,2,7*]

Environmental boundaries anchor cognitive maps that support memory. However, trapezoidal boundary geometry distorts the regular firing patterns of entorhinal grid cells, proposedly providing a metric for cognitive maps. Here we test the impact of trapezoidal boundary geometry on human spatial memory using immersive virtual reality. Consistent with reduced regularity of grid patterns in rodents and a grid-cell model based on the eigenvectors of the successor representation, human positional memory was degraded in a trapezoid environment compared with a square environment—an effect that was particularly pronounced in the narrow part of the trapezoid. Congruent with changes in the spatial frequency of eigenvector grid patterns, distance estimates between remembered positions were persistently biased, revealing distorted memory maps that explained behaviour better than the objective maps. Our findings demonstrate that environmental geometry affects human spatial memory in a similar manner to rodent grid-cell activity and, therefore, strengthen the putative link between grid cells and behaviour along with their cognitive functions beyond navigation.

Boundaries are essential for navigators moving through space, and boundary geometry serves as a strong cue for reorientation[1,2]. When rodents and human children are disoriented after learning the location of a hidden reward, they search for the reward equally often in geometrically equivalent corners of rectangular environments[3–5]. Consistent with this, human adults rely on boundary geometry for spatial updating, which is facilitated by the limited number of symmetry axes of the enclosure boundaries[6]. The learning of positions relative to a boundary, which recruits the hippocampal formation, is thought to occur incidentally[7,8] and positions closer to a boundary are remembered more accurately than those further away from it[9].

Here we examined the possibility that boundary geometry can cause distortions in human spatial memory. We derive this hypothesis from the distortions induced by environmental geometry on the grid-cell firing patterns in rodents[10–12]. Grid cells, which were first identified in the entorhinal cortex of freely moving rodents, typically exhibit sixfold periodic (hexadirectional) spatial firing that extends across the environment[13]. This pattern can be described in terms of its scale, as well as its offset and orientation relative to the environment[13,14]. Along the dorsoventral axis of the medial entorhinal cortex, grid cells that share similar spacing and orientations are organized in discrete modules[15–17]. Grid cells have been directly recorded in human patients undergoing presurgical screening[18,19], and—in human functional magnetic resonance imaging (fMRI) studies—hexadirectional signals serve as a proxy measure for activity of the entorhinal grid system[20]. However, empirical evidence demonstrating the behavioural relevance of grid cells remains scarce.

Theoretical work suggests that regular grid patterns provide a compact code for self-localization and function as a metric of space, supporting path integration and vector-based navigation[13,14,21–27]. Thus, location is encoded by the conjunction of spatial phases across different modules—the population phase[25,28]—whereas the distance and direction between points can be derived from the relative difference in population phase[25]. With a regular underlying grid pattern, there should be a tight coupling between the distance separating positions and the change in grid population phase. Larger distances in space correspond to greater changes in the population phase of the grid.

Environmental geometry strongly influences grid firing patterns in rodents[10–12,29]. Changes made to the geometry of a familiar enclosure produce commensurate changes to the scale of grid patterns, resulting in differential rates of change in population phase for travel in the changed and unchanged dimension[15,17]. Similar manipulations made while humans navigate in virtual reality (VR) environments produce complementary deficits in path integration[30]. Notably, in highly polarized enclosures such as trapezoids, grid patterns are highly distorted and less regular than in square control enclosures[10]. These changes are especially pronounced in the narrow part of the trapezoidal enclosure with reduced symmetry, less regular fields and a change of grid orientation—changes that do not appear to attenuate with continued exposure[10]. Similarly, in a quadrilateral environment with one slanted wall, firing fields of grid cells were consistently shifted away from the slanted wall, resulting in a local distortion of the grid[11]. Together, these findings indicate not only that environmental boundaries anchor spatial representations, but also that the specific arrangement of environmental boundaries can distort spatial codes in the mammalian brain. However, research into the potential consequences of compromised grid patterns for human spatial cognition is lacking.

Here we investigated how environmental geometry—which is known to distort grid-cell-based computations—influences human

[1]Max Planck Institute for Human Cognitive and Brain Sciences, Leipzig, Germany. [2]Kavli Institute for Systems Neuroscience, Centre for Neural Computation, The Egil and Pauline Braathen and Fred Kavli Centre for Cortical Microcircuits, Norwegian University of Science and Technology, Trondheim, Norway. [3]Donders Institute for Brain, Cognition and Behaviour, Radboud University, Nijmegen, the Netherlands. [4]Institute of Behavioural Neuroscience, University College London, London, UK. [5]Research Department of Cell and Developmental Biology, University College London, London, UK. [6]Amsterdam Brain and Cognition, University of Amsterdam, Amsterdam, The Netherlands. [7]These authors contributed equally: Caswell Barry, Christian F. Doeller.
*e-mail: bellmund@cbs.mpg.de; doeller@cbs.mpg.de

spatial cognition. Degraded grid patterns in a trapezoid are hypothesized to carry less precise positional information than regular grid patterns, resulting in uncertainties about locations in space and the distances between them[10,11,28]. We therefore investigated the effects of boundary geometry on human spatial memory. We captured the effects of environmental geometry on grid patterns using the eigenvectors of the successor representation (SR; see Methods), which has been previously related to reinforcement learning and choice behaviour[31–35]. The eigenvectors of the SR exhibit grid-like properties in two-dimensional space, the regularity of which is degraded in a trapezoid[32]. We demonstrate that distorted eigenvector grid patterns convey less-precise information about self-location in a trapezoid and that this effect is most pronounced at the narrow end of the trapezoid environment. We tested whether memory for object positions is impaired in a trapezoid compared with a square control environment. Within the trapezoid, we expected worse memory performance, particularly in the narrow part of the enclosure compared with the broad part. Moreover, spatial computations performed on the basis of distorted grid patterns are expected to exhibit systematic biases. SR grid patterns were, on average, stretched in the trapezoid relative to the square and compressed in the narrow part of the trapezoid compared with the broad part. We asked participants to judge distances between remembered locations and contrasted their estimates of identical true distances as a function of environmental geometry.

Results

Positional memory. We used immersive VR to investigate the effects of environmental geometry on human spatial memory (Fig. 1a). Wearing a head-mounted display (HMD), the participants navigated different environments using a motion platform that translated real-world rotations and steps into virtual movement (Fig. 1b). The participants were familiarized with the VR setup in a circular environment before learning object positions in a square and a trapezoid with the order of environments counterbalanced across participants. The environments were of equal surface area, and distinct wall colours served as orientation cues. During the object-position memory task, the participants learned the positions of six objects in each environment; the object positions were organized into two triplets with matched inter-object distances in both halves of an environment (Fig. 1c). The participants were tested on the positions of the objects after an initial learning phase by having to navigate to the remembered position of a cued object in each trial (Fig. 1d). To probe mnemonic distortions outside the encoding environment, the participants judged pairwise distances between object positions in VR by walking the distance in the circular familiarization environment and on a computer screen by adjusting a slider on a subjective scale.

Does the disruption of regular grid patterns (Fig. 1e,f and Extended Data Fig. 1; two-sample t-test of grid similarity across environment halves, $t_{98}=10.81$, $P<0.001$, Cohen's $d=2.14$, 95% confidence interval (CI): 1.83–2.61) result in less accurate positional codes? To test this notion, we used a Bayesian decoder to decode locations using synthetic spike trains sampled from a population of SR grid patterns ($n=50$), which were derived from the eigenvectors of successor representations from the square and trapezoid environment. Decoding was performed using a simple maximum-likelihood approach assuming uniform priors[36]. Decoding errors—the displacement between the true and decoded position—were larger in the trapezoid than in the square (Fig. 1g; two-sample t-test, $t_{58}=117.41$, $P<0.001$, $d=29.93$, 95% CI = 26.06–37.00), indicating that distorted grid patterns carry less positional information. To exclude the possibility that this reduction simply reflected the change in environmental aspect ratio, we verified that decoding accuracy for the smallest possible rectangular environment that entirely encloses the trapezoid exceeds the decoding accuracy for the trapezoid itself (Extended Data Fig. 2; two-sample t-test, $t_{58}=64.52$, $P<0.001$, $d=16.44$, 95% CI = 14.29–20.46). Thus, distorted grid patterns indeed underlie reduced positional decoding in the trapezoid.

Is human positional memory also degraded in a trapezoid? First, we compared raw positional-memory error—the displacement between the response and correct position—between the two environments. Consistent with the degradation of positional information observed in simulated grid patterns, the participants made larger errors in the trapezoid than the square (Fig. 2a; bootstrapped paired t-test, $t_{36}=2.71$, $P<0.001$, $d=0.45$, 95% CI = 0.16–0.73; we analysed the behavioural data using bootstrap-based t-tests and report bootstrapped confidence intervals of the effect size throughout; see Methods). To ensure that this effect was not due to the fact that the trapezoid allows larger errors owing to its elongated shape, we calculated memory scores that accounted for differences in the distribution of possible errors for each position[37]. We generated a chance distribution of 1,000 random locations that uniformly covered the entire environment and quantified the distance of each random location to the correct positions, resulting in a specific distribution of possible error distances for each position. For each trial, we calculated the memory score as 1 − the proportion of distances from the chance distribution smaller than the replacement error. This yielded a score ranging from 0 (low memory) to 1 (perfect memory) for each trial, taking into account the range of possible errors based on the correct position and environmental geometry (the overall distribution of memory scores is provided in Extended Data Fig. 4a). Importantly, memory scores were significantly lower in the trapezoid compared with the square (Fig. 2b,c; bootstrapped paired t-test, $t_{36}=-2.30$, $P<0.001$, $d=-0.38$, 95% CI = −0.67 to −0.08), ensuring that decreased positional memory was not due to different distributions of possible errors as a result of the elongated shape of the trapezoid.

In rodents, grid patterns recorded from a trapezoid are known to be more strongly distorted in the narrow end of the environment than its base[10]. Similarly, we found that decoding errors derived from SR grid patterns were also larger in the narrow part of the trapezoid (Fig. 1h; two-sample t-test, $t_{58}=14.63$, $P<0.001$, $d=3.73$, 95% CI = 3.12–4.82). To determine whether human spatial memory differed within the trapezoid, we examined memory errors and found, as expected, that errors were larger in the narrow end (Fig. 2d; bootstrapped paired t-test, $t_{31}=2.75$, $P<0.001$, $d=0.49$, 95% CI = 0.19–0.82). To control for the expected difference in error distributions, we again calculated memory scores and confirmed a robust difference between the two ends of the environment (Fig. 2e; bootstrapped paired t-test, $t_{31}=-1.59$, $P=0.023$, $d=-0.28$, 95% CI = −0.61–0.06). The difference in positional-memory errors between the narrow and broad parts of the trapezoid was higher than the 5th percentile of a surrogate distribution of error differences obtained by comparing positional memory between the halves of the square, indicating a significant difference between the environments (Extended Data Fig. 4c; Z-statistic = 2.18, $P=0.015$). Taken together, the profile of positional memory observed is in line with our predictions derived from deformations of grid patterns with degraded positional memory in the trapezoidal environment compared with the square environment and more impaired performance in the narrow part of the trapezoid than the broad part. Indeed, calculating the Bayes factor to quantify the likelihood of observing differences in positional memory between environments and trapezoid halves on the basis of the decoding errors of the SR grid model compared with a null model of no difference revealed strong evidence for the SR grid model ($BF_{10}=23.58$; we report twice the natural logarithm of the Bayes factor throughout; see Methods).

During our task, in the absence of other positional cues, object locations had to be learned relative to the enclosure boundaries. Can differences in boundary proximity explain the pattern of results in line with more accurate memory for positions near boundaries[9]?

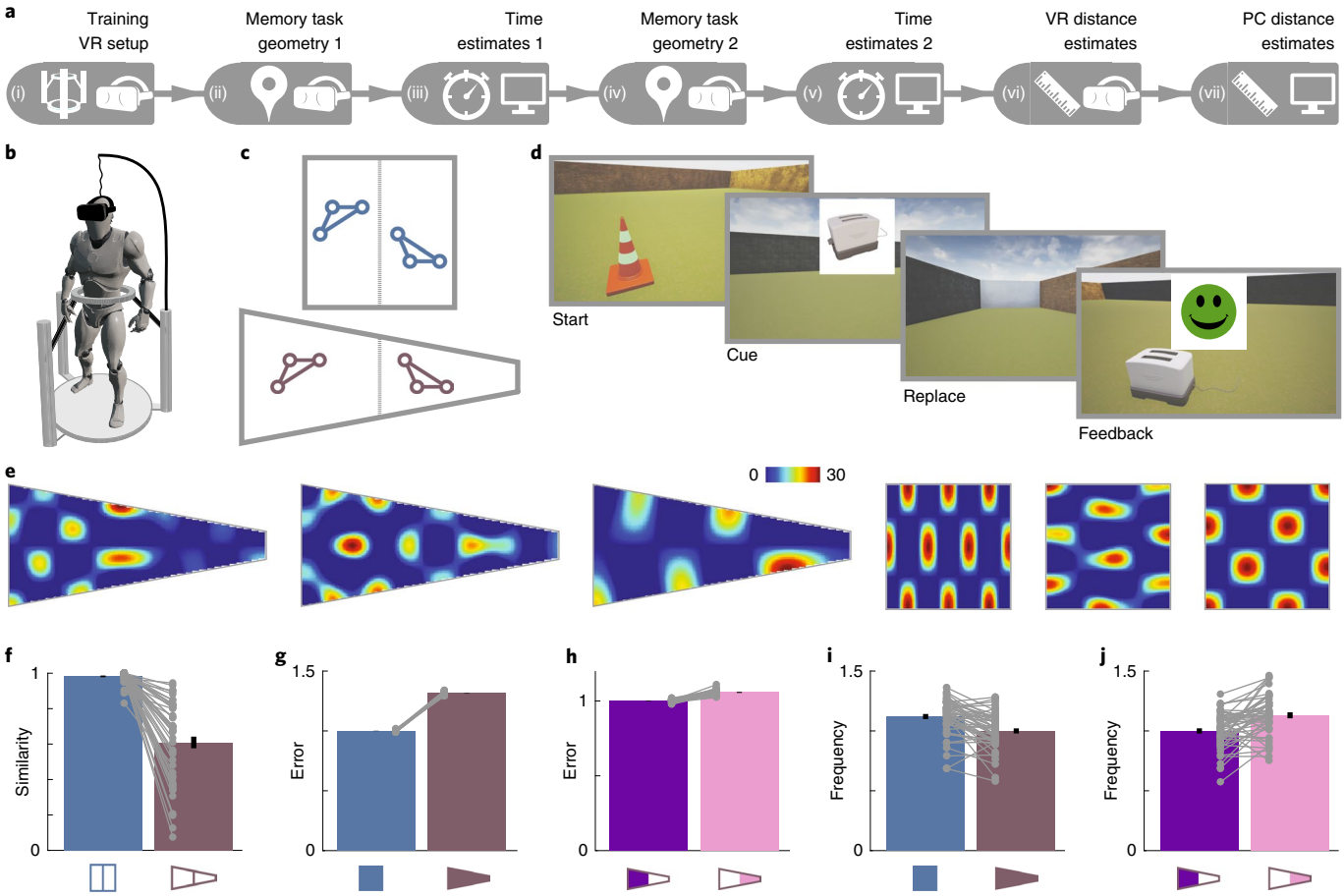

Fig. 1 | Task design and SR grid patterns. a, The experimental timeline. The participants were familiarized with the VR setup (i) before completing the object-position memory task (ii and iv) followed by time estimates (iii and v) in the two environments. The participants subsequently estimated pairwise distances between the positions learned in VR and on a computer screen (vi and vii). The headset and screen icons indicate whether individual tasks took place in VR or on a computer screen, respectively. **b**, Schematic of the immersive VR setup with an HMD and a motion platform, which translated physical steps and rotations into virtual movement. **c**, An example configuration of object positions (circles). Two triplets of objects were positioned in each environment with one triplet in each half of each environment, yielding four triplets with matched distances between positions. **d**, To commence a test trial in the object-position memory task, participants walked to a start position, which was marked by a pylon, where they were cued with the image of an object. Subsequently, the participant navigated to the object's remembered position, which they indicated by pressing a button, and received feedback. **e**, Example eigenvector grid patterns of the successor representation for a trapezoid (left; Extended Data Fig. 1a) and a square (right; Extended Data Fig. 1b) environment. **f**, SR grid patterns are distorted in the trapezoid, resulting in reduced correlation coefficients of spatial autocorrelations between the two trapezoid halves compared with the halves of the square. **g**,**h**, Position decoding errors based on spikes sampled from SR grid patterns are larger in the trapezoid than in the square (**g**) and larger in the narrow part of the trapezoid than the broad part (**h**), demonstrating that distorted grid patterns carry less positional information (Extended Data Fig. 2). **i**,**j**, Mean radial frequencies of SR grid patterns are lower in the trapezoid than in the square (**i**) and higher in the narrow part of the trapezoid than the broad part (**j**; Extended Data Fig. 3). For **f**–**j** data are mean ± s.e.m.; symbols indicate experimental conditions for which data is shown. Individual data points reflect iterations (**g** and **h**) or SR grid patterns (**f**, **i** and **j**).

Owing to the specific geometry of the trapezoid, distances of object positions to the closest boundary were smaller in the trapezoid than in the square (bootstrapped paired t-test, $t_{36}=-10.09$, $P<0.001$, $d=-1.66$, 95% CI = −2.23 to −1.30) and smaller in the narrow part of the trapezoid compared with the broad part (bootstrapped paired t-test, $t_{36}=-18.34$, $P<0.001$, $d=-3.02$, 95% CI = −4.05 to −2.44). Thus, the boundary proximity model predicts better memory in the trapezoid and the narrow end of this environment—directly opposite to the effects that we predicted and observed. Congruent with the beneficial role of boundary proximity, distances to the closest boundary were negatively correlated with memory scores in the square (Extended Data Fig. 4e; bootstrapped one-sample t-test, $t_{36}=-4.42$, $P<0.001$, $d=-0.73$, 95% CI = −1.15 to −0.40). In the trapezoid, however, there was no statistically significant effect of boundary proximity on memory scores (bootstrapped one-sample t-test, $t_{36}=-0.40$, $P=0.524$, $d=-0.07$, 95% CI = −0.39–0.27; bootstrapped paired t-test of difference between square and trapezoid, $t_{36}=-3.45$, $P<0.001$, $d=-0.57$, 95% CI = −0.96 to −0.26), suggesting a differential relationship of boundary proximity and positional memory in non-rectangular environments.

Differences in positional memory in both environments were not due to differential navigation behaviour. There were no statistically significant differences in the excess path lengths of participants' navigation paths from the start position of a given trial to the remembered location of the object in the trapezoid environment compared with the square environment or between the two parts of the trapezoid (Extended Data Fig. 5a,b; bootstrapped paired t-tests, square versus trapezoid: $t_{36}=-0.95$, $P=0.144$, $d=-0.16$, 95% CI = −0.48–0.18; broad versus narrow trapezoid: $t_{36}=-0.11$, $P=0.865$, $d=-0.02$, 95% CI = −0.31–0.36). Furthermore, there were no statistically significant differences in walking speeds between the two environments or the sub-parts of the trapezoid

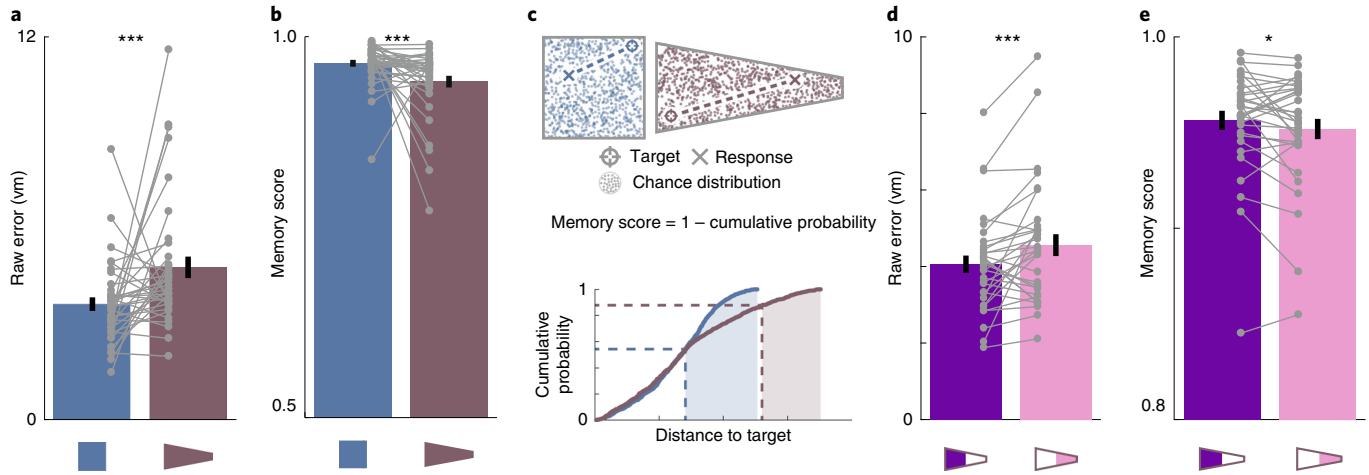

Fig. 2 | Distorted positional memory in the trapezoid. a, Positional-memory errors in virtual metres (vm), measured as the Euclidean distance between the correct and remembered position, were larger for object positions in the trapezoid than in the square environment. **b**, Similarly, memory scores were lower in the trapezoid than in the square environment. The *y* axis was thresholded at the chance level of 0.5. **c**, Schematics of the expression of positional memory using memory scores to control for differences in distributions of possible errors for two hypothetical trials. For both environments, a chance distribution of positions uniformly covering the available space was generated (top, coloured dots). We quantified the cumulative probability of the chance distribution as a function of distance to target object positions (bottom). Positional-memory performance of a given trial was then expressed as 1 – the cumulative probability at the error distance between the true and response position, resulting in memory scores ranging from 0 to 1, for which 0.5 represents chance level performance and 1 represents perfect performance. Conceptually, this corresponds to the proportion of the chance distribution that is further away from the correct position than the remembered position (shaded areas). **d**, Raw positional-memory errors were larger in the narrow part of the trapezoid compared with the broad part. Five participants were excluded owing to differences between broad and narrow part of more than 1.5× the interquartile range above or below the upper and lower quartile of differences, respectively. The full dataset is provided in Extended Data Fig. 4b. **e**, Similarly, memory scores were lower in the narrow part of the trapezoid than the broad part. The *y* axis was thresholded to illustrate the difference between conditions. For **a**, **b**, **d** and **e**, data are mean ± s.e.m. The grey circles indicate individual participant data with lines connecting data points from the same participant. Note that graphs in **b** and **e** do not start at 0. $^{*}P < 0.05$, $^{***}P < 0.001$.

(Extended Data Fig. 5c,d; bootstrapped paired *t*-tests, trapezoid versus square: $t_{36} = -0.01$, $P = 0.973$, $d = 0.00$, 95% CI = −0.33–0.34; broad versus narrow trapezoid: $t_{36} = 1.15$, $P = 0.079$, $d = 0.19$, 95% CI = −0.14–0.51). There was no statistically significant relationship between Euclidean distances from the start positions to the correct object positions and spatial-memory performance (Extended Data Fig. 5e,f; bootstrapped one-sample *t*-tests, square: $t_{36} = 0.17$, $P = 0.764$, $d = 0.03$; 95% CI = −0.32–0.35; trapezoid: $t_{36} = 0.58$, $P = 0.358$, $d = 0.10$, 95% CI = −0.22–0.46; trapezoid broad: $t_{36} = 1.37$, $P = 0.177$, $d = 0.23$, 95% CI = −0.10–0.65; trapezoid narrow: $t_{36} = -0.01$, $P = 0.987$, $d = 0.00$, 95% CI = −0.36–0.32).

To investigate the navigation behaviour of the participants in more detail, we next examined their body and head orientation during the replacement period relative to the direction from start to response position in each trial. Both body and head orientation of participants were significantly clustered around the directions from the start to response positions in the square (*v*-tests, body: $v = 36.84$, $P < 0.001$; head: $v = 36.68$, $P < 0.001$) and in the trapezoid (*v*-tests, body: $v = 36.89$, $P < 0.001$; head: $v = 36.68$, $P < 0.001$), and there was no statistically significant effect of environment on the distributions of mean orientations (Extended Data Fig. 6a,b; Watson–Williams tests, body: $F_{1,72} = 0.02$, $P = 0.889$; head: $F_{1,72} = 0.14$, $P = 0.709$). Similar results were obtained for the body and head orientations when comparing trials targeting objects in the broad and narrow parts of the trapezoid (Extended Data Fig. 6c,d; *v*-test, body broad: $v = 36.73$, $P < 0.001$; *v*-test, body narrow: $v = 36.73$, $P < 0.001$; Watson–Williams test, difference body: $F_{1,72} = 1.53$, $P = 0.220$; *v*-test, head broad: $v = 36.54$, $P < 0.001$; *v*-test, head narrow: $v = 36.65$, $P < 0.001$; Watson–Williams test, difference head $F_{1,72} = 0.05$, $P = 0.830$). We therefore do not think that the average facing direction of participants influences our key comparisons between the two environments or within the trapezoid. There was no statistically significant difference in the circular variance around each trial's average body direction between environments (Extended Data Fig. 6e; trapezoid versus square: bootstrapped paired *t*-test, $t_{36} = 1.06$, $P = 0.118$, $d = 0.17$, 95% CI = −0.16–0.46) or the trapezoid parts (Extended Data Fig. 6g; narrow versus broad: bootstrapped paired *t*-test, $t_{36} = 1.14$, $P = 0.076$, $d = -0.19$, 95% CI = −0.13–0.54), but the circular variance of participants' facing directions was greater in the trapezoid than in the square (Extended Data Fig. 6f; bootstrapped paired *t*-test, $t_{36} = 2.57$, $P < 0.001$, $d = 0.42$, 95% CI = 0.13–0.73) and greater in the narrow part of the trapezoid than the broad part (Extended Data Fig. 6h; bootstrapped paired *t*-test, $t_{36} = 2.13$, $P < 0.001$, $d = 0.35$, 95% CI = 0.04–0.69). This suggests that the participants relied more on visual exploration of the environment, decoupled from body rotations and chosen trajectories in our VR setup. Taken together, we observed no credible evidence of participants being generally disoriented in the trapezoid or of fundamental differences in navigational strategies between environments. The object-position memory task was designed to probe memory for positions in the broad and narrow parts of the trapezoid rather than to evenly sample the environment. Participants therefore more frequently faced towards the narrow or broad end of the trapezoid when navigating towards remembered positions in the respective part of the environment (Extended Data Fig. 7a; *v*-tests, broad: $v = 31.84$, $P < 0.001$; narrow: $v = 28.50$, $P < 0.001$). Furthermore, the velocity of participants was higher along the long axis of the trapezoid (Extended Data Fig. 7b; *v*-tests, broad: $v = 27.03$, $P < 0.001$; narrow: $v = 13.51$, $P = 0.001$). Do attentional resources and task demands differ between test environments? This seems unlikely as our design included a secondary task in which the participants memorized colour changes of an extramaze cue and later estimated the durations between colour-change events (see Methods). There were no statistically significant differences between square

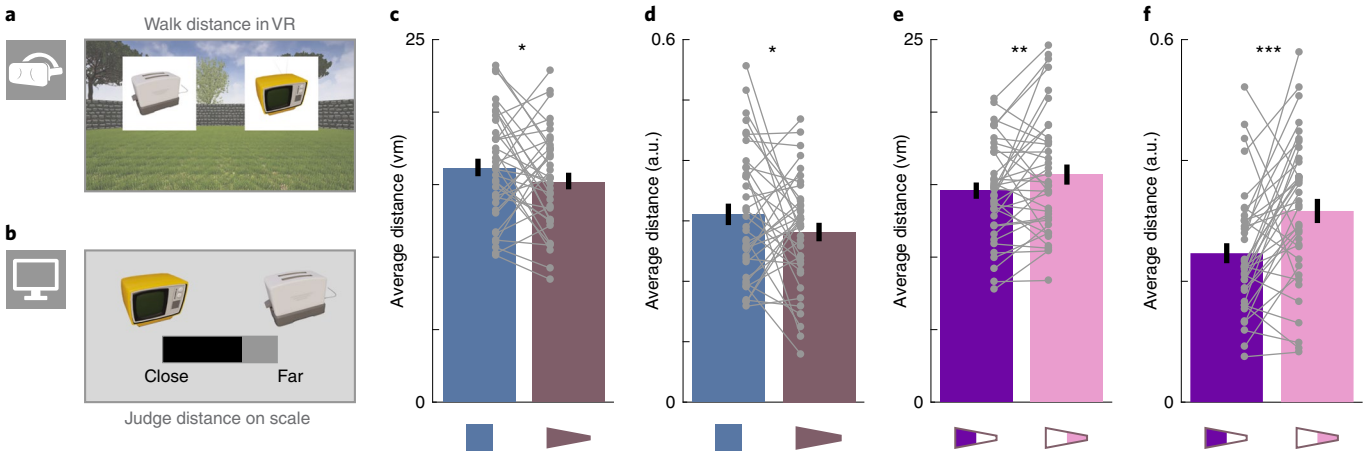

Fig. 3 | Distortion of distance estimates. a, The participants were cued to estimate and walk distances between the remembered positions of object pairs in a circular virtual environment. **b**, In the desktop version of the task, the participants adjusted a slider to estimate the distance between object pairs on a subjective scale from close together to far apart. **c**,**d**, Taking advantage of matched distances between object positions, estimated distances were averaged and compared between environments. Distances were estimated to be shorter in the trapezoid than in the square in both the VR (**c**) and desktop (**d**) version of the task, in line with the lower radial frequencies of the SR grid patterns in the trapezoid (Fig. 1i, Extended Data Fig. 3a). **e**,**f**, Identical distances were estimated to be longer in the narrow part of the trapezoid than in the broad part for judgements made in VR (**e**) and on a computer screen (**f**), consistent with the more tightly packed SR grid patterns in the narrow part of the trapezoid (Fig. 1j, Extended Data Fig. 3b). For **c**–**f**, data are mean ± s.e.m. The grey circles indicate individual participant data. $^{**}P < 0.01$.

and trapezoid (Extended Data Fig. 10) in mean estimation errors (bootstrapped paired *t*-test, $t_{36} = -0.10$, $P = 0.873$ $d = -0.02$, 95% CI = −0.37–0.31) and absolute estimation errors (bootstrapped paired *t*-test, $t_{36} = -0.32$, $P = 0.629$, $d = -0.05$, 95% CI = −0.37–0.29) or the error variability (bootstrapped paired *t*-test, $t_{36} = -0.81$, $P = 0.205$, $d = -0.13$, 95% CI = −0.46–0.19).

Mnemonic distortions outside the environment. We next addressed whether computations based on spatial memories that are distorted through environmental geometry are systematically biased outside the learning environment. We therefore asked participants to estimate distances between the positions of object pairs in two modalities, after the object-position memory tasks (Fig. 3a,b). In the VR version of the distance-estimation task, the participants reported distances by walking the respective distance between two remembered object positions in a circular enclosure, which was different from the original square and trapezoidal environments. In the desktop version of this task, the participants indicated these distances on a subjective scale using a computer mouse (see Methods). The participants successfully completed both versions of the task (Extended Data Fig. 8a,b; bootstrapped paired *t*-test of long versus short distances in VR version, $t_{36} = 11.00$, $P < 0.001$, $d = 1.81$, 95% CI = 1.38–2.53; mean ± s.d. of Spearman correlations between true and estimated distances in desktop version, $r = 0.67 \pm 0.19$), demonstrating the ability to compute never-experienced distances from pairs of remembered positions. Comparison of the distances walked in the VR version of the task to true Euclidean distances across all of the trials revealed an overestimation bias (bootstrapped paired *t*-test, $t_{36} = 5.78$, $P < 0.001$, $d = 0.95$, 95% CI = 0.60–1.47).

How could distorted grid patterns during encoding bias later distance estimates? The entorhinal grid system is thought to be a central component of the neural substrate that supports vector-based navigation, which enables the calculation of navigational vectors by comparing the grid population phases of positions[22,25,27,38,39]. In such a system, the difference in grid population phase between locations is expected to be proportional to the Euclidean displacement between them[25,28]. Thus, for a participant to make accurate distance judgements, the relationship between the Euclidean distance and grid phase distance must be held constant in both the presentation and response context. If, for example, a distance was encoded with a population of grid patterns that had been compressed (increased frequency) then attempts to recapitulate that distance with unbiased grid patterns would result in an overestimation in Euclidean space. To determine whether successor-based grid patterns were systematically distorted in either the square or trapezoid environment, we applied a Fourier approach. Specifically, an analysis of the spatial frequency of the SR grid rate maps revealed a sparser packing of grid fields in the trapezoid than the square (Fig. 1i, Extended Data Fig. 3a; two-sample *t*-test, $t_{98} = 3.98$, $P < 0.001$, $d = 0.79$, 95% CI = 0.39–1.25; see Methods). Thus, grid phase changed more slowly as a function of distance in the trapezoid, which might result in underestimations of distances relative to the square[28].

Taking advantage of our design in which participants learned a triplet of object positions in each half of an environment with matched inter-object distances, we compared distance estimates between environments. In line with stretched SR grid patterns, distances were judged to be shorter in the trapezoid than in the square in both the VR (Fig. 3c; bootstrapped paired *t*-test, $t_{36} = 1.44$, $P = 0.025$, $d = 0.24$, 95% CI = −0.08–0.61) and the desktop (Fig. 3d; bootstrapped paired *t*-test, $t_{36} = 1.49$, $P = 0.027$, $d = 0.24$, 95% CI = −0.07–0.56) version of the task. This effect was highly reliable between the two versions of the task (Extended Data Fig. 8c; Spearman $r = 0.79$, $P < 0.001$, 95% CI of correlation coefficient: 0.61–0.88). Next, we tested for a difference between distance estimates for the two parts of the trapezoid. Consistent with higher frequencies of the successor-based grid patterns in the narrow part of the trapezoid compared with the broad part (Fig. 1j, Extended Data Fig. 3b; two-sample *t*-test, $t_{98} = 3.90$, $P < 0.001$, $d = 0.78$, 95% CI = 0.39–1.21), the participants estimated that the same distances were longer in the narrow part of the trapezoid than in the broad part (Fig. 3e,f; VR: bootstrapped paired *t*-test, $t_{36} = 2.09$, $P = 0.002$, $d = 0.34$, 95% CI = 0.03–0.68; desktop: bootstrapped paired *t*-test, $t_{36} = 3.46$, $P < 0.001$, $d = 0.57$, 95% CI = 0.22–1.05). Again, the difference between remembered distances was highly correlated across the two modalities (Extended Data Fig. 8d; Spearman $r = 0.70$, $P < 0.001$, 95% CI of correlation coefficient: 0.36–0.89). We calculated surrogate distributions of distance differences between the two halves of the square to contrast the two environments.

In both versions of the task, the distance difference of the trapezoid halves differed significantly from the surrogate distributions of distance differences obtained from the square halves (Extended Data Fig. 8e,f; VR: $Z=4.05$, $P<0.001$; desktop: $Z=3.68$, $P<0.001$). These findings demonstrate that—across two versions of the task with very different response formats—distance estimates for identical distances are systematically biased in a manner that is consistent with the spatial frequencies of distorted SR grid patterns in the trapezoid. We assessed the likelihood of observing longer distance estimates in the square and in the narrow end of the trapezoid, given differences in spatial frequency of the SR grid patterns. Again, the Bayes factor strongly favoured the SR grid model over the null model (VR: $BF_{10}=15.31$; desktop: $BF_{10}=18.68$).

Reconstruction of remembered locations. What is the structure of deformed memory maps? To reconstruct remembered object positions from estimated inter-object distances, we applied multidimensional scaling (MDS) to the data obtained in the desktop version of the task (Fig. 4a). We extracted coordinates along two dimensions (Extended Data Fig. 9a), which we mapped onto the true coordinates of the trapezoid using Procrustes analysis to match the two configurations of the coordinates (Fig. 4a, Extended Data Fig. 9b; see Methods). We quantified the deviance between the true and reconstructed positions after Procrustes analysis and compared this Procrustes distance to a surrogate distribution of distances that were obtained by shuffling object-position assignments to assess the statistical significance of the reconstruction accuracy (Fig. 4b). The observed Procrustes distances were significantly lower than the 5th percentiles of the surrogate distributions (Fig. 4c; bootstrapped paired t-test, $t_{36}=-8.48$, $P<0.001$, $d=-1.39$, 95% CI $=-2.26$ to -0.89), reflecting a close match between true and reconstructed positions. Importantly, recalculating the above-described memory scores using the reconstructed positions led to higher scores compared with the true positions (Fig. 4d; bootstrapped paired t-test, $t_{36}=3.09$, $P<0.001$, $d=0.51$, 95% CI $=0.18$–0.95), providing direct evidence that positional memory is used to compute distances between objects and that distorting the spatial map also distorts distance estimates. This effect was also found to be significant when we excluded trials that targeted objects for which the reconstructed position lay outside the environment (bootstrapped paired t-test, $t_{36}=1.42$, $P=0.023$, $d=0.23$, 95% CI $=-0.08$–0.64). The increase in memory scores could be explained if, for each position, reconstructed positions reflect remembered positions in the trapezoid. To quantify this, we calculated the error vectors between the true and remembered positions in the object-position memory task and compared these to the error vectors of the reconstructed positions. We observed a strong relationship between the two sets of error vectors as indicated by a significant correlation of their average lengths (Fig. 4e; Pearson $r=0.62$, $P<0.001$, 95% CI of correlation coefficient: 0.33–0.79) and a clustering of their orientations (Fig. 4f; angular difference of vectors significantly clustered around 0, v-test, $v=13.77$, $P=0.001$). These findings show that positions

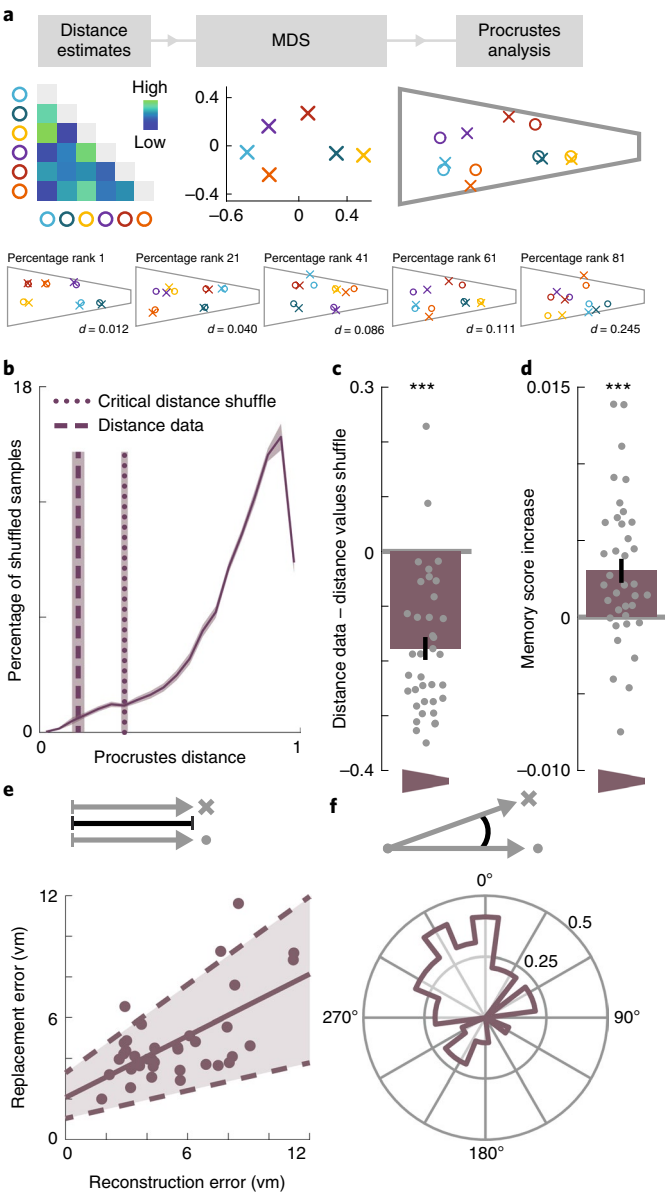

Fig. 4 | Reconstruction of remembered positions. a, Top: using MDS, coordinates along two underlying dimensions were extracted from pairwise distance estimates. The resulting coordinates were mapped to the original object positions in the trapezoid using Procrustes analysis (see Methods). The colour bar indicates estimated distances. Data are shown for a randomly selected participant. Bottom: the five participants chosen to show reconstruction accuracy across the sample on the basis of the spread of Procrustes distances (data shown for participants at percentile ranks 1, 21, 41, 61 and 81, from left to right). The coloured circles indicate correct positions and the crosses the respective reconstructed positions. **b**, The Procrustes distance quantifies the deviation between the true positions and the reconstructed positions as the normalized sum of squared error distances. The mean across participants is indicated by a dashed vertical line. For each participant, a surrogate distribution of Procrustes distances was obtained by fitting the coordinates from MDS to coordinate sets with shuffled object identities (solid line). The dotted vertical line indicates the averaged critical Procrustes distance, defined as the 5th percentile of the respective surrogate distributions. The shaded areas indicate s.e.m. across participants. **c**, The Procrustes distances from fitting to true coordinates were significantly smaller than the critical distances of the surrogate distributions. **d**, Memory scores quantifying positional memory within the environment were significantly higher when calculated with respect to the reconstructed object positions rather than the true object positions. **e**, The average error vector lengths from the object-position memory task correlate across participants with error vector lengths of the positions reconstructed from distance estimates. The circles show individual participant data, the solid line indicates the least squares line and the dashed lines and shaded region indicate bootstrapped confidence intervals. **f**, The angular differences in orientation between the two sets of error vectors cluster around 0°, indicating that errors were shifted in the same direction. For **c** and **d**, data are mean ± s.e.m. The grey circles indicate individual participant data.

reconstructed on the basis of distance estimates were shifted in the same direction as remembered positions and that the magnitude of this shift corresponded to the size of the errors in the object-position memory task.

Discussion

Here we used immersive VR to demonstrate that environmental geometry can distort human spatial memory. Our data show that positional memory is impaired in a trapezoid environment compared with a square environment and that the deficits are most pronounced in the narrow end of the trapezoid environment. These findings are consistent with environmentally induced distortions observed in rodent entorhinal grid patterns. Equally, they closely mirror predictions drawn from a model grid-cell system derived from the eigenvectors of the SR. Importantly, mnemonic distortions persisted outside the environment—participants estimated identical distances to be different between the square and trapezoid environments as well as between the narrow and broad parts of the trapezoid, underscoring an effect of environmental geometry during encoding on subsequent memory, in line with spatial frequencies of SR grid patterns. Moreover, remembered positions that were reconstructed from these distance estimates directly reflected positional memory during the learning task.

Our findings demonstrate that environmental geometry has a strong impact on human spatial memory. We predicted this influence from rodent data in which the sixfold symmetry of grid firing is distorted in a trapezoidal enclosure, with the most pronounced distortions in the narrow part of the enclosure[10]. We show degraded positional memory as a function of environmental geometry, in line with larger position decoding errors based on the eigenvector grid patterns of the SR, as well as with impaired positional decoding from simulated grid cells with locally distorted firing patterns[11]. Together with evidence for impaired path integration with disrupted grid-cell firing in rodents[40] and increased path integration errors in older adults with weaker hexadirectional signals measured with fMRI[41], previous studies support the interpretation that the integrity of the grid pattern is beneficial for human spatial memory. The strength of hexadirectional signals and the directional coherence of the orientation of these signals across voxels in the entorhinal cortex are associated with memory performance across participants who are learning object positions in circular enclosures[20,42]. Our findings dovetail with this notion as they demonstrate that environmental geometry, which is known to compromise grid patterns in rodents, influences spatial cognition in a within-subject design.

We further demonstrate that distortions persist beyond the encoding environment. The grid-cell population phase is thought to provide a mechanism to encode spatial positions and calculate vectors between locations[25]. As such, distortions of the grid pattern can decouple the rate of change in population phase from distance in the environment[28]. Two positions separated by a given distance will be encoded more similarly when grid patterns are of lower rather than higher spatial frequency. When estimating distances between positions, more-similar grid population phases will result in shorter distance estimates[22,25,27,38,39]. Consistent with the lower spatial frequencies of SR grid patterns, the participants estimated identical distances to be shorter in the trapezoid than in the square. Within the trapezoid, SR grid patterns had a higher spatial frequency in the narrow end and, consistent with this, participants estimated distances to be greater in the narrow part of the trapezoid compared with the broad part.

Our results show that human spatial memory was distorted in a trapezoidal environment, suggesting that boundary geometry can distort mnemonic representations. Previous studies have investigated the role of trapezoidal boundary geometry for spatial updating and reorientation. Evidence suggests that trapezoid room geometry can be used successfully for spatial updating in the absence of additional orientation cues. A limited number of symmetry axes was suggested to facilitate the maintenance of the orientation of a person in angular environments, in contrast to circular environments[6]. Consistent with this, human participants successfully rely on trapezoidal boundary geometry for heading retrieval[43,44]. In our task, wall textures provided additional unambiguous non-geometric cues for orientation in both environments, making it unlikely that participants were disoriented in either the square or the trapezoid environments[5,44]. This supports our interpretation that the effects reflect differences in positional memory rather than being driven by disorientation or differences in navigation behaviour. Learning positions relative to environmental boundaries recruits the hippocampal formation and is thought to occur incidentally[7,8]. Recent evidence suggests that positions near a boundary are remembered more accurately than positions in the centre of a rectangular enclosure[9]. Although we replicate the finding that boundary proximity is beneficial for positional memory in the square, this cannot explain the pattern of results we observed. Positions in the trapezoid were closer to the nearest boundary than in the square and, within the trapezoid, positions in the narrow part were closer to a boundary than in the broad part. Our findings suggest that boundaries can also distort human spatial memory, in line with grid pattern distortions through environmental geometry.

Previous studies suggested that changing environmental boundaries might influence human spatial cognition in ways that are consistent with the findings from studies of rodent place[45] and grid cells[13]. Focusing on path integration, which is one of the core functions assumed for grid cells[13,14,21], biases in human navigation have been reported to follow predictions derived from grid-cell firing[30]. In particular, the experimental design in Chen et al.[30] built on the observation that rodent grid patterns rescale to match changes made to the geometry of already familiar enclosures[15]. Expansions and compressions of boundaries relative to preceding trials resulted in under- and overshoots of the return path in a path integration task, when the path included a component along the manipulated boundary dimension[30]. This illustrates how, through environmental change, altering the rate of change in grid-cell population phase in relation to distance travelled can introduce biases in human navigation[28,30]. As described above, translating this idea to the memory-based estimation of distances between locations might explain the diverging judgements of identical distances observed in our data. Expansions and compressions of virtual environments have further been demonstrated to impact spatial memory in humans and, under conditions of environmental change, positional memory follows models of place cells and boundary proximity[46,47]. Whereas the studies described above indicate how boundary manipulations in familiar environments influence spatial behaviour, we built on work showing that distorted grid patterns persist in static trapezoid environments even with prolonged experience[10]. Our findings suggest that distortions of the spatial metric of the brain can result in mnemonic distortions under constant boundary conditions within a specific environment and even outside of this encoding environment.

We opted for a purely behavioural experiment; however, our hypotheses, experimental design and analysis directly built on findings from electrophysiological recordings of grid cells in rodents[10]. We used highly immersive VR technology to enhance the impact of environmental geometry on spatial cognition and engage proprioceptive, vestibular and motor systems during the task. At present, immersive VR does not allow the concurrent recording of neural data. The contribution of locomotor cues to the experience of navigation in general has been emphasized previously[48] and recent studies in rodents have used gain manipulations in VR to emphasize the contributions of locomotor cues to grid-cell firing specifically[49,50]. Having established the impact of environmental geometry on human spatial cognition, an exciting question for future research

would be to combine manipulations of environmental geometry with neuroimaging techniques such as fMRI to study the deformations of the cognitive map that we describe here in the brain. To do so, an important measure could be the hexadirectional signal that can be observed in the human entorhinal cortex[20]. Beyond fMRI, an exciting future avenue is created by the development of new magnetoencephalography systems, which might enable the combination of immersive VR with recordings of neural data[51].

As large parts of human indoor navigation take place in rectangular rooms, the novelty of a trapezoidal enclosure in our task might be considered to be a factor that contributed to impaired performance compared with the square. However, such an effect of unfamiliarity with polarized environments would not predict the observed within-environment differences in performance. Furthermore, we did not observe statistically significant differences in the walking speeds of participants between environments or in the directness of their paths from the start to the remembered object positions. Thus, none of our control measures provided credible evidence for fundamental differences in navigational performance between the environments by themselves. Moreover, we observed no credible evidence that the environmental manipulation affected the detection and encoding of colour-change events, arguing against an effect of increased task demand in the trapezoid environment as sufficient attentional resources were available for this secondary task.

Importantly, the effects that we observed in positional memory persisted outside the environment as demonstrated by the differential estimates for matched distances between positions within the different parts of the trapezoid. These distortions were highly reliable across response modalities, demonstrating a general, task-invariant mnemonic effect. Our findings agree with asymmetric distance judgements between landmarks and non-landmarks as well as overestimations of distances as a function of intermediary boundaries[52–57]. Beyond boundaries separating positions, our findings demonstrate that distance estimates can be influenced through the geometric arrangement of boundaries. The response profiles observed in the VR version of the task revealed a general tendency to overestimate distances between positions, consistent with previous studies that report overestimations of navigated distances[58] and spatial scale in map drawings[59]. We used the distances that were estimated on a subjective scale in the desktop version of the task to reconstruct remembered positions. Accounting for the distortions in the memory of the participants by using these reconstructed positions to recompute memory scores yielded increased performance scores. This illustrates the close match between positions reconstructed from distance estimates and positional memory within the environment, and demonstrates that—consistent with the formation of cognitive maps[60]—distances that were never directly experienced in the task were computed from remembered positions. Grid cells have been suggested to support this kind of vector computation[25,27]. This is further in line with evidence for the involvement of the entorhinal grid system in imagination[61,62] and theoretical accounts that propose a role for spatially tuned cells in memory[63–65].

Environmental geometry systematically biased memory-based computations outside the trapezoid environment, thereby linking our findings to a growing body of literature that implicates grid-cell computations in cognitive functions beyond navigation[66]. For example, grid-like hexadirectional signals were also observed during trajectories through an abstract feature space, which was spanned by the dimensions of neck and leg length of stick figure birds[67]. Collectively, these findings indicate a role of the entorhinal grid system in mapping cognitive spaces[66]. As proposed for navigable space[13,14,21,25,26], the regular firing patterns of grid cells might provide a metric for these spaces, enabling the efficient encoding of specific stimuli located at different positions within a space. Speculatively, correlated feature dimensions or feature spaces in which subsets of feature combinations are impossible might distort how grid cells map these spaces in a similar way as environmental geometry distorts grid-cell firing patterns, resulting in biased representations similar to the distortions of spatial memory observed in this study.

In conclusion, our data show distortions of human spatial memory that are consistent with the changes induced in rodent grid-cell activity by the geometry of highly polarized enclosures. These distortions persist outside the environment, indicating that environmental geometry has an enduring impact on memory. In line with the proposed roles for grid cells in navigation and mapping feature dimensions beyond navigable space, these findings suggest that environmental geometry might be able to distort the metric of cognitive representations.

Methods

Participants. We recruited 53 participants between the age of 18 and 30 from the Norwegian University of Science and Technology. All of the participants provided written informed consent before participation, and all of the research procedures were approved by the regional ethics committee (REC North, 2017/153). The participants were compensated for their time at a rate of kr100 per hour. The sample size was determined on the basis of a power calculation assuming a small to medium effect ($d = 0.4$) of environmental geometry on human spatial cognition, and resulting in a sample size of 52 to achieve a statistical power of 80% ($\alpha = 0.05$, two-tailed test). A total of 39 participants (mean age 23.8 ± 2.5 years, 36% female) completed the experiment (14 incomplete datasets due to technical difficulties with the VR setup or motion sickness). Two participants were excluded owing to poor memory performance, which was defined as average replacement errors of more than 1.5× the interquartile range larger than the upper quartile of average errors in the sample. Thus, 37 participants entered the analyses.

Overview. We designed our experiment to test distortions of spatial memory as a function of environmental geometry. An overview of the experimental structure is provided in Fig. 1a. The participants were first familiarized with the VR setup (Fig. 1a, (i)) before beginning the object-position memory task in the first environment. The object-position memory task (Fig. 1a, ii and iv) was performed in a trapezoidal or square environment for 20 min each, and the order of environments was counterbalanced across participants. After navigating an environment, the participants were prompted to estimate the durations between occasional colour-change events encountered in that environment (Fig. 1a, iii and v). In the final two tasks, the participants were asked to estimate the distances between pairs of objects in VR and on a computer screen (Fig. 1a, vi and vii), respectively. The design of each task and the corresponding analyses are described in detail in the sections below. All of the analyses were performed using MATLAB (release 2017a, MathWorks) and statistical tests (two-tailed unless stated otherwise; $\alpha = 0.05$) were performed using resampling procedures as implemented in EEGLAB[68]. Specifically, test statistics were compared against a surrogate distribution obtained from 10,000 bootstrap samples respecting within-participant dependencies. Respecting the dependent nature of our data, Cohen's d was calculated as the mean difference divided by the s.d. of the difference scores (compare with equation 6 in ref. [69]) and the 95% CIs of this effect size were bootstrapped (10,000 iterations) using the Measures of Effect Size Toolbox[70]. Circular statistics were implemented using the MATLAB-based Circular Statistics Toolbox[71]. Data collection and analysis were not performed blind to the conditions of the experiments.

Virtual reality. Aiming to maximize the feeling of immersion and, therefore, the impact of environmental features, we used state-of-the-art VR technology consisting of an HMD (Oculus Rift CV1) and a motion platform (Cyberith Virtualizer). The participants wore low-friction overshoes and were strapped into a harness attached to the motion platform's ring system, allowing free rotations. To navigate the virtual environments, the participants were instructed to lean slightly into the ring construction to slide the front foot backwards across the sensors of the low-friction base plate of the motion platform while taking a step forward with the back foot (Supplementary Video 1), generating translational movement in the current forward direction determined by the orientation of the participant in the ring system[72]. Head movements were tracked in three dimensions using the HMD's tracking system and the virtual environments were displayed to both eyes separately at a resolution of 1,080 × 1,200 px and a refresh rate of 90 Hz. The virtual environments were created and presented using the Unreal Engine (v.4.13.2, Epic Games, 2017) and the eye height of the participants was set to 1.80 vm. The participants were familiarized with the VR setup in a circular environment (45.74 vm in diameter), which consisted of a grass floor that was curtailed by a wall (height 3.75 vm). A set of trees that were spread around the outside of the environment served as cues for orientation. During familiarization, the participants practiced walking and turning by navigating the circular environment to collect coins that appeared at random positions in the environment. The participants were

instructed to walk towards the coins and collect them through button presses on a handheld controller. Moreover, this familiarization period served as a practice for the time-estimation task (see below).

Object-position memory task. The participants performed an object-position memory task, during which they iteratively learned the positions of six objects in a trapezoidal environment (36 vm × 76 vm × 8 vm × 76 vm); the lengths of the sides were proportional to the enclosure that rodents explored in a previous study that reported distortions of grid-cell firing patterns[10]. To establish a behavioural baseline, the participants also performed this task in a square control environment (40.27 vm × 40.27 vm) with an equal surface area. To enforce spatial learning on the basis of environmental geometry, there were no distal cues outside the environment. To facilitate orientation, each wall was presented in a unique colour. Both environments had a grass floor, and a blue sky with moving clouds was visible (Fig. 1b). The participants performed the task for 20 min in each environment, and the order was counterbalanced across participants. In each environment, the participants learned the positions of six everyday objects, which were presented as three-dimensional models. The assignment of objects to arenas and positions was randomized across participants.

In each trial of an initial learning phase, the participants navigated to a start position, which was indicated by a traffic cone. An object was then shown at its predefined position in the environment and the participants were instructed to navigate to the object, collect it by button press and memorize its position. Each object was shown once and the order of objects was randomized. In the subsequent test phase (Fig. 1b), the participants again navigated to start positions. On arrival at the start position, a picture of one of the objects was shown as a cue for 3 s in front of the participant, prompting the participants to navigate to where they remembered this object was in the environment. The participants indicated the remembered position by button press after arrival and received feedback about their accuracy in the form of one of five smiley faces. The object then appeared at its correct position and the participants collected it before the beginning of the next trial. The participants completed 30.54 ± 6.71 and 30.38 ± 8.09 (mean ± s.d.) test trials in the square and trapezoid environments, respectively, and there was no statistically significant difference between environments in the number of trials (bootstrapped paired t-test, $t_{36} = 0.18$, $P = 0.759$).

The order of trials was randomized for mini-blocks of six trials so that, within a mini-block, each object was sampled once and no two consecutive trials sampled the same objects. A triplet of object positions (Fig. 1c) was randomly generated for each participant with a minimum distance of 11 vm between object positions and a minimum of at least 3 vm to the nearest boundary. Positions were constrained so that the connection between two objects was parallel to the long axis of the trapezoid or one of the walls of the square. The third object was placed at an angle ranging from 90° to 120° relative to the first two with the same distance to one of the objects as between the first two. Such a triplet of positions was placed in both the narrow and broad parts of the trapezoid, defined on the basis of the midpoint of its long axis and the left and right parts of the square. Placing triplets of objects with matched distances in each part of the environment enabled direct comparisons of remembered distances between environments and their sub-parts (see the 'Distance-estimation tasks' section). As cues were only shown after participants arrived at the start position of a given trial, the participants never walked the direct path between two objects. There were no statistically significant relationships between the distance from start positions to target object positions (mean ± s.d., square: 18.66 ± 4.65 vm; trapezoid: 19.92 ± 8.50 vm; trapezoid broad: 21.10 ± 10.95 vm; trapezoid narrow: 18.73 ± 4.67 vm) and spatial memory performance (Extended Data Fig. 5e,f).

Positional memory. Raw positional-memory errors were quantified as the Euclidean distance between the correct position of an object in the environment and the position remembered by the participant. To limit the influence of outlier trials, we excluded trials with errors larger than 1.5× the interquartile distance above the upper quartile of errors for each participant (mean ± s.e.m. number of trials excluded per participant = 3.35 ± 0.26) from all further analyses. Average positional-memory errors were compared across environments using a bootstrap-based paired t-test (Fig. 2a). To account for the fact that, despite the equal area, larger errors are possible in the trapezoid compared with the square control environment, we subsequently quantified performance using memory scores. Specifically, we generated a distribution of 1,000 random locations uniformly covering each environment and, for each trial, quantified the proportion of locations that were further away from the correct object position than the position indicated by the participant. Importantly, calculating memory scores on the basis of the distribution of possible errors for each target position yields a measure that is comparable across positions and environments[37] with a chance level of 0.5 for random performance and scores closer to 1 for high performance. To test the hypothesis of degraded spatial memory in the trapezoid, memory scores were compared across environments using a bootstrap-based paired t-test (Fig. 2b).

Next, we aimed to test the more specific hypothesis of increased degradation of positional memory in the narrow part of the trapezoid compared with the broad part, derived from the larger distortions of firing patterns of grid cells in this part of the environment[10]. We used a bootstrap-based t-test to test whether positional-memory errors differed between the narrow and broad parts of the trapezoid (Fig. 2d). Outlier participants were excluded on the basis of our standard criterion of values more than 1.5× the interquartile range above or below the upper or lower quartile, respectively (the full dataset is provided in Extended Data Fig. 4b). Distributions of possible errors can differ also for positions within the same environment. We therefore also tested whether memory scores differed between the two parts of the trapezoid (Fig. 2e).

As the rotationally symmetrical geometry of the square does not predefine how to calculate the difference in positional memory, we created a surrogate distribution by shuffling which half of the environment was to serve as the subtrahend and minuend for the error difference across participants. For each permutation, we calculated the error difference for objects located in the two halves of the square. The positional-memory error difference observed in the trapezoid was smaller than the 5th percentile (one-tailed test) of the surrogate distribution obtained from 10,000 permutations (Extended Data Fig. 4c). The shape of the surrogate distribution did not differ statistically from normality (Kolmogorov–Smirnov test, $D = 0.01$, $P = 0.277$); we therefore used the inverse of the normal cumulative distribution function to convert the P value reflecting the number of occurrences of smaller memory ratios in the surrogate distribution into a Z-statistic. To visualize response behaviour in the two parts of the trapezoid, we collapsed across all trials from all of the participants for objects located in the broad and narrow parts of the arena. Response positions were centred on the respective true positions and divided into 50 × 50 square bins with a side length of 0.6 vm. The resulting histogram was smoothed using a Gaussian kernel with an s.d. of 0.5 vm and plotted as a heat map (Extended Data Fig. 4d). To test the influence of the distance to the nearest boundary on positional memory, we calculated the Pearson correlation between the Euclidean distance to the closest boundary and the memory scores across all of the trials from an environment for each participant. We tested the resulting correlation coefficients against 0 and between the environments using bootstrap-based t-tests. Negative correlation coefficients indicate better memory closer to the boundary.

Parameters of navigation. To assess whether differences in navigation behaviour might underlie the observed differences in positional memory, we analysed navigational performance in the replacement phase of each trial, in which participants navigated to the remembered position of a cued object. For each trial, we calculated the Euclidean distance between the start position and the response location, and subtracted it from the length of the path walked by the participant. This excess path length measures the directness of the paths taken, potentially reflecting the degree of certainty about the trajectory as increased uncertainty might lead to more turns and longer paths. We contrasted averaged excess path lengths between the two environments and the broad and narrow parts of the trapezoid (Extended Data Fig. 5a,b). Similarly, we contrasted average walking speeds during the replacement phase between the environments and trials targeting objects from the two trapezoid parts (Extended Data Fig. 5c,d).

We also assessed whether the distance from a trial's start position was related to the accuracy of object-position memory in a consistent way across subjects. For each participant, we calculated the Spearman correlation coefficient between the distances from start to true object positions and positional memory as defined by the Euclidean distances between true and remembered object positions. The resulting coefficients were tested against 0 for all of the trials in the square and the trapezoid environments separately (Extended Data Fig. 5e) or for trials analysing objects in the narrow and broad parts of the trapezoid (Extended Data Fig. 5f).

Next, we assessed the rotations that participants made during the replacement phase of the trial. To achieve this, we centred the rotation of the body, as measured by the orientation of the motion platform's ring construction, and the orientation of the participant's head, as tracked by the HMD, on the direction from start to response position. We averaged orientation values for trials within the square and trapezoid environments, or the broad and narrow parts of the trapezoid, and tested for clustering around 0° using v-tests and differences in averaged orientation values between conditions using Watson–Williams tests[71] (Extended Data Fig. 6, top). Furthermore, we quantified the circular variance of centred orientation values and contrasted it across conditions (Extended Data Fig. 6, bottom). None of these measures suggested that navigation behaviour alone had influenced the key conclusions of the paper.

Furthermore, we tested the sampling of directions separately for trials targeting objects in the narrow and broad parts of the trapezoid. For each of 36 angular bins with a width of 10°, we computed the proportion of time points during which participants' bodies faced the direction of that bin. We averaged these proportions across participants for the polar histogram in Extended Data Fig. 7a. To test whether angular sampling was biased towards the long and short base of the trapezoid, we calculated the angular mean for each participant and used v-tests to test for a clustering around 180° and 0°, respectively. We next quantified average movement velocity for each direction bin (Extended Data Fig. 7b). We weighted directions by average velocity to compute a circular mean for each participant. Again, we tested using v-tests whether the resulting circular means clustered around 180° and 0° for trials in which target objects were located in the broad and narrow parts of the environment, respectively.

Distance-estimation tasks. After completing the time-estimation task following the second object-position memory task in the second environment, the participants estimated distances between pairs of object positions in two modalities: on a computer screen and by walking the actual distances in VR.

Virtual reality. The participants were placed in the same circular virtual arena as the familiarization session. Each trial began with an arrow pointing to the middle of the arena, with the arrow appearing at a random location on the arena floor. After the participants positioned themselves on the base of the arrow, images of two objects were presented in front of them for 3 s (Fig. 3a). The participants were instructed to walk the distance that they remembered the objects to be apart on the basis of the object-position memory task while following the direction indicated by the arrow. When the participants terminated a trial by button press, a checkmark was presented to indicate the successful registration of the response and the next trial began. Owing to time constraints, this task was restricted to distances between objects within a triplet, resulting in 12 trials making up a block. The trial order within blocks was randomized with the constraint that trials with objects from the two environments alternated. The participants completed two blocks with a short break in between.

As only the distances within a triplet of positions were tested during this task, participants' averaged estimates for the long and short distances were compared using a bootstrap-based paired *t*-test as an indicator of successful task performance (Extended Data Fig. 8a). To test whether distance estimates for the same distances differed between environments or the narrow and broad parts of the trapezoid, we took advantage of the fact that true distances were matched across position triplets and, therefore, across environment parts. The distance estimates for the two triplets within an environment were averaged and contrasted between the square and trapezoid using bootstrap-based *t*-tests (Fig. 3c). Similarly, response distances within a triplet were averaged and compared between the narrow and the broad parts of the trapezoid using bootstrap-based *t*-tests (Fig. 3e). As for the difference in positional memory, we created a surrogate distribution to compare the difference in distance estimation observed between the trapezoid halves and the square by shuffling across participants which half of the square was to serve as the minuend and subtrahend for the distance difference in each of 10,000 permutations. The distance difference observed in the trapezoid was more extreme than the 2.5th and 97.5th percentiles (two-tailed test) of this surrogate distribution (Extended Data Fig. 8e). The shape of the surrogate distribution did not differ statistically from normality (Kolmogorov–Smirnov test, $D=0.01$, $P=0.200$).

Computer monitor. Afterwards, the participants were instructed to estimate distances between object pairs on a desktop computer setup. Images of objects on a white background, as well as an adjustable horizontal bar with the labels 'close together' on the left and 'far apart' on the right were presented on a computer screen (Fig. 3c). Again, participants were instructed to estimate how far objects were apart during the object-location memory task. Here, they indicated their response by adjusting the horizontal bar using a computer mouse, after which a grey screen was shown for 500 ms. All of the possible combinations of distances were analysed, that is, including comparisons across triplets, yielding subjective distances between all pairs of object positions in an environment. Each of the 15 combinations of object pairs per environment was probed twice, resulting in a total of 60 trials. The trial order was randomized with the constraint that each possible pair of objects was sampled before any object combination was sampled for the second time. Each object was shown once on the left and once on the right side of the screen in the two trials sampling a given object pair. This distance-estimation task, as well as the time-estimation task, was presented using the Psychophysics Toolbox[73] for MATLAB (release 2016a). General performance in this task was assessed by calculating Spearman correlations between the estimated distances and the respective true distances (Extended Data Fig. 8b). Furthermore, the distance estimates were contrasted between environments and between the narrow and broad parts of the trapezoid as described above. The surrogate distribution obtained for comparison to the square did not differ statistically from normality (Kolmogorov–Smirnov test, $D=0.01$, $P=0.167$).

Reconstructing remembered positions. To reconstruct the positions of remembered objects in the trapezoid from distance estimates, MDS was applied to the distance estimates that were obtained in the desktop version of the task, as distances were estimated between all pairs of positions only in the desktop version of the task. The estimated distances were normalized to a range from 0 to 1 and averaged across the two repetitions of each object pair and subjected to MDS to recover coordinates that reflected this distance structure using metric stress as the cost function and a random initial configuration of points. Our approach assumed that two dimensions underlie the object location memory formed during the navigation task. To assess whether this assumption holds, we compared the model deviance of general linear models predicting the distances between true positions from the positions recovered from MDS for different numbers of dimensions. As expected, unexplained variance was substantially decreased when using two instead of one dimension, but no clear improvement resulted from a larger number of dimensions (Extended Data Fig. 9).

To match the coordinates that resulted from MDS to the original positions in the virtual environment, we used Procrustes analysis, which enabled translation, scaling, reflection and rotation (an application of the combination of MDS and Procrustes analysis to fMRI data was described previously[74]). The goodness of fit, the Procrustes distance, was quantified by the normalized sum of squared errors between the reconstructed and true coordinates, and was compared with Procrustes distances that resulted from the Procrustes analyses of the MDS coordinates and sets of coordinates in which the assignment of object identity to position was shuffled, yielding a surrogate distribution from all 720 possible permutations. Specifically, we tested on the group level whether the fits between reconstructed coordinates and true coordinates were better than the fits constituting the 5th percentile (reflecting the threshold for statistical significance at $\alpha=0.05$) of each participant's surrogate distribution (Fig. 4b,c). The reconstructed coordinates are shown as heat maps (Extended Data Fig. 9b) following the same procedure as described above.

To test whether the reconstructed positions indeed reflected participants' memory in the object-position memory task, we recalculated the memory scores as described above but with the coordinates resulting from the Procrustes analysis instead of the true object positions as goal positions (Fig. 4d). To rule out that the effect was driven by objects for which positions were reconstructed to be remembered outside of the environment, we excluded all of the affected trials from the memory score calculation in an additional control analysis. To describe the overlap between positions reconstructed from distance estimates and performance in the object-position memory task, we calculated error vectors on the basis of the true object positions for both the reconstructed positions and the response positions from the object-position memory task. Specifically, we tested whether error vectors were of a similar length and had a similar orientation to demonstrate that positions were shifted by a similar distance and in a similar direction. We quantified the match between average error vectors of response and reconstructed positions by correlating their lengths using Pearson correlation (Fig. 4e). We further analysed the similarity in orientation of these error vectors by averaging the angular differences between vectors from the correct to the respective response and reconstructed positions for each participant and testing the resulting circular means for a clustering around 0° using a *v*-test (Fig. 4f).

Time-estimation task. To probe whether attentional demands differed between environments, we included a secondary task while participants performed the object-position memory task. If attentional demand differed across environments, we would expect to see differences in the performance of the secondary task. In the sky above each arena, a ring was presented that changed colour four times during the object-position memory task per environment. The ring remained in a given colour for an interval between 2 min and 6 min and the participants indicated colour changes by button presses and were instructed to remember the order of colours and the duration of the presentation of each colour. Although different colours were presented in the two environments, the intervals between colour changes were constant across environments, allowing for a comparison of temporal memory between square and trapezoid environments.

After completing the object-position memory task in an environment, the participants were placed in front of a computer screen to estimate the time between colour changes before continuing with the next part of the experiment (Fig. 1a). On a white screen, two pairs of consecutive colours were shown and the participants indicated the time interval that they remembered between the two colour changes in minutes and seconds, for example, how much time passed between the ring changing colour from blue to yellow and changing from yellow to green. The participants were cued to estimate the time between all six possible combinations of colour changes per environment. To ensure full understanding of this task, the participants estimated intervals between colour changes occurring at random times every 30 s to 120 s during the familiarization phase before the object-position memory task. Overall performance in this task was quantified using Spearman correlations between the correct and estimated time intervals before specifically comparing average estimation errors, absolute estimation errors and the s.d. of estimation errors across environments (Extended Data Fig. 10).

Successor representation grid patterns. Following Stachenfeld et al.[32], simulated grid cells were generated using the first 50 non-constant eigenvectors of the SR matrix under a uniform random-walk policy for a square (90 × 90 cm) and a trapezoid (length 187 cm, parallel walls 90 cm and 20 cm, based on Krupic et al.[10]). Eigenvectors were thresholded at zero and scaled to a peak firing rate of 30 Hz. To assess the distortion of SR grid fields within the trapezoidal environment, we divided the square and trapezoid environments into halves across the longest axis and computed the spatial autocorrelation of the SR grid rate maps on each half. Grid similarity was then calculated by taking the Pearson correlation between the autocorrelations from each half of the environment (Fig. 1f). As the shortest dimension of the trapezoid was 20 spatial bins, a circular window of radius 40 spatial bins was used to compare the autocorrelations ensuring the window for comparison never went off the autocorrelation map.

The decoding analysis sampled each spatial bin (1 cm^2) of the environment 30 times. On each occasion, for each of the 50 cells, spikes were randomly generated for a 100 ms time window according to a Poisson process with rate parameters

equal to the SR grids' firing rates in that bin. The locations were then decoded using the maximum likelihood estimate of all 50 SR grid spike counts, and errors were calculated as the Euclidean distance between the true and decoded locations[36,75] (Fig. 1g,h). Decoding errors were normalized so that errors in the square environment and broad part of the trapezoid had a mean of 1 for the comparison between environments and trapezoid halves, respectively.

To analyse differences in the spatial frequencies of the SR grids, we calculated the two-dimensional fast Fourier transform (FFT) for each rate map and reparametrized the FFT into polar coordinates. Power spectra were then considered solely as a function of radial frequency by averaging across the angular component of the FFT (Extended Data Fig. 3). Finally, we calculated the mean radial frequency of each SR grid and compared these across and within environments (Fig. 1i,j). Statistical significance of all SR grid pattern analyses was assessed using standard two-sample *t*-tests. The bias-corrected difference between means divided by the pooled s.d. served as the effect size and is reported with bootstrapped 95% confidence intervals[70].

Likelihood analyses were performed separately for both the positional-memory and distance-estimation tasks. For each task, the proportional differences in participants' responses from the square-trapezoid and within-trapezoid contrasts were compared to the distribution of proportional differences expected by the SR model. The same was performed for a null model using the same distribution of proportional differences as the SR, but with a shifted mean to predict no overall difference in the square-trapezoid and within-trapezoid contrasts. Likelihoods from the square–trapezoid and within-trapezoid contrasts were combined within tasks to give the likelihood of the human responses given each of the models for both the positional memory and distance-estimation tasks. The Bayes factor BF_{10} was calculated as the ratio between the two model likelihoods. We report twice the natural logarithm of the Bayes factor ($2\ln(BF_{10})$) as it has a similar scale to familiar likelihood ratio test statistics[76]. According to the conventions by Kass and Raftery[76], $2\ln(BF_{10}) > 10$ constitutes very strong evidence for the alternative over the null model.

Reporting Summary. Further information on research design is available in the Nature Research Reporting Summary linked to this article.

Data availability

The data that support the findings of this study are available from the corresponding authors on reasonable request.

Code availability

The custom code that supports the findings of this study is available from the corresponding authors on reasonable request.

Received: 6 August 2018; Accepted: 4 October 2019;
Published online: 18 November 2019

References

1. Cheng, K. & Newcombe, N. S. Is there a geometric module for spatial orientation? Squaring theory and evidence. *Psychon. Bull. Rev.* **12**, 1–23 (2005).
2. Julian, J. B., Keinath, A. T., Marchette, S. A. & Epstein, R. A. The neurocognitive basis of spatial reorientation. *Curr. Biol.* **28**, R1059–R1073 (2018).
3. Cheng, K. A purely geometric module in the rat's spatial representation. *Cognition* **23**, 149–178 (1986).
4. Margules, J. & Gallistel, C. R. Heading in the rat: determination by environmental shape. *Anim. Learn. Behav.* **16**, 404–410 (1988).
5. Hermer, L. & Spelke, E. S. A geometric process for spatial reorientation in young children. *Nature* **370**, 57–59 (1994).
6. Kelly, J. W., McNamara, T. P., Bodenheimer, B., Carr, T. H. & Rieser, J. J. The shape of human navigation: how environmental geometry is used in maintenance of spatial orientation. *Cognition* **109**, 281–286 (2008).
7. Doeller, C. F. & Burgess, N. Distinct error-correcting and incidental learning of location relative to landmarks and boundaries. *Proc. Natl Acad. Sci. USA* **105**, 5909–5914 (2008).
8. Doeller, C. F., King, Ja & Burgess, N. Parallel striatal and hippocampal systems for landmarks and boundaries in spatial memory. *Proc. Natl Acad. Sci. USA* **105**, 5915–5920 (2008).
9. Lee, S. A. et al. Electrophysiological signatures of spatial boundaries in the human subiculum. *J. Neurosci.* **38**, 3265–3272 (2018).
10. Krupic, J., Bauza, M., Burton, S., Barry, C. & O'Keefe, J. Grid cell symmetry is shaped by environmental geometry. *Nature* **518**, 232–235 (2015).
11. Krupic, J., Bauza, M., Burton, S. & O'Keefe, J. Local transformations of the hippocampal cognitive map. *Science* **359**, 1143–1146 (2018).
12. Stensola, T., Stensola, H., Moser, M.-B. & Moser, E. I. Shearing-induced asymmetry in entorhinal grid cells. *Nature* **518**, 207–212 (2015).
13. Hafting, T., Fyhn, M., Molden, S., Moser, M.-B. & Moser, E. I. Microstructure of a spatial map in the entorhinal cortex. *Nature* **436**, 801–806 (2005).
14. Moser, E. I., Moser, M.-B. & McNaughton, B. L. Spatial representation in the hippocampal formation: a history. *Nat. Neurosci.* **20**, 1448–1464 (2017).
15. Barry, C., Hayman, R., Burgess, N. & Jeffery, K. J. Experience-dependent rescaling of entorhinal grids. *Nat. Neurosci.* **10**, 682–684 (2007).
16. Brun, V. H. et al. Progressive increase in grid scale from dorsal to ventral medial entorhinal cortex. *Hippocampus* **18**, 1200–1212 (2008).
17. Stensola, H. et al. The entorhinal grid map is discretized. *Nature* **492**, 72–78 (2012).
18. Jacobs, J. et al. Direct recordings of grid-like neuronal activity in human spatial navigation. *Nat. Neurosci.* **16**, 1188–1190 (2013).
19. Nadasdy, Z. et al. Context-dependent spatially periodic activity in the human entorhinal cortex. *Proc. Natl Acad. Sci. USA* **114**, E3516–E3525 (2017).
20. Doeller, C. F., Barry, C. & Burgess, N. Evidence for grid cells in a human memory network. *Nature* **463**, 657–661 (2010).
21. McNaughton, B. L., Battaglia, F. P., Jensen, O., Moser, E. I. & Moser, M.-B. Path integration and the neural basis of the 'cognitive map'. *Nat. Rev. Neurosci.* **7**, 663–678 (2006).
22. Fiete, I. R., Burak, Y. & Brookings, T. What grid cells convey about rat location. *J. Neurosci.* **28**, 6858–6871 (2008).
23. Burak, Y. & Fiete, I. R. Accurate path integration in continuous attractor network models of grid cells. *PLoS Comput. Biol.* **5**, e1000291 (2009).
24. Mathis, A., Herz, A. V. M. & Stemmler, M. Optimal population codes for space: grid cells outperform place cells. *Neural Comput.* **24**, 2280–2317 (2012).
25. Bush, D., Barry, C., Manson, D. & Burgess, N. Using grid cells for navigation. *Neuron* **87**, 507–520 (2015).
26. Herz, A. V., Mathis, A. & Stemmler, M. Periodic population codes: from a single circular variable to higher dimensions, multiple nested scales, and conceptual spaces. *Curr. Opin. Neurobiol.* **46**, 99–108 (2017).
27. Banino, A. et al. Vector-based navigation using grid-like representations in artificial agents. *Nature* **557**, 429–433 (2018).
28. Carpenter, F. & Barry, C. Distorted grids as a spatial label and metric. *Trends Cogn. Sci.* **20**, 164–167 (2016).
29. Sun, C. et al. Distinct speed dependence of entorhinal island and ocean cells, including respective grid cells. *Proc. Natl Acad. Sci. USA* **112**, 9466–9471 (2015).
30. Chen, X., He, Q., Kelly, J. W., Fiete, I. R. & McNamara, T. P. Bias in human path integration Is predicted by properties of grid cells. *Curr. Biol.* **25**, 1771–1776 (2015).
31. Dayan, P. Improving generalization for temporal difference learning: the successor representation. *Neural Comput.* **5**, 613–624 (1993).
32. Stachenfeld, K. L., Botvinick, M. M. & Gershman, S. J. The hippocampus as a predictive map. *Nat. Neurosci.* **20**, 1643–1653 (2017).
33. Momennejad, I. et al. The successor representation in human reinforcement learning. *Nat. Hum. Behav.* **1**, 680 (2017).
34. Russek, E. M., Momennejad, I., Botvinick, M. M., Gershman, S. J. & Daw, N. D. Predictive representations can link model-based reinforcement learning to model-free mechanisms. *PLoS Comput. Biol.* **13**, e1005768 (2017).
35. Gershman, S. J. The successor representation: its computational logic and neural substrates. *J. Neurosci.* **38**, 7193–7200 (2018).
36. Towse, B. W., Barry, C., Bush, D. & Burgess, N. Optimal configurations of spatial scale for grid cell firing under noise and uncertainty. *Proc. R. Soc. B* **369**, 20130290 (2014).
37. Jacobs, J. et al. Direct electrical stimulation of the human entorhinal region and hippocampus impairs memory. *Neuron* **92**, 983–990 (2016).
38. Kubie, J. L. & Fenton, A. A. Linear look-ahead in conjunctive cells: an entorhinal mechanism for vector-based navigation. *Front. Neural Circuits* **6**, 20 (2012).
39. Erdem, U. M. & Hasselmo, M. A goal-directed spatial navigation model using forward trajectory planning based on grid cells: forward linear look-ahead trajectory model. *Eur. J. Neurosci.* **35**, 916–931 (2012).
40. Gil, M. et al. Impaired path integration in mice with disrupted grid cell firing. *Nat. Neurosci.* **21**, 81–91 (2018).
41. Stangl, M. et al. Compromised grid-cell-like representations in old age as a key mechanism to explain age-related navigational deficits. *Curr. Biol.* **28**, 1108–1115 (2018).
42. Kunz, L. et al. Reduced grid-cell–like representations in adults at genetic risk for Alzheimer's disease. *Science* **350**, 430–433 (2015).
43. Sturz, B. R., Gurley, T. & Bodily, K. D. Orientation in trapezoid-shaped enclosures: implications for theoretical accounts of geometry learning. *J. Exp. Psychol.* **37**, 246–253 (2011).
44. Twyman, A. D., Holden, M. P. & Newcombe, N. S. First direct evidence of cue integration in reorientation: a new paradigm. *Cogn. Sci.* **42**, 923–936 (2018).
45. O'Keefe, J. & Dostrovsky, J. The hippocampus as a spatial map. Preliminary evidence from unit activity in the freely-moving rat. *Brain Res.* **34**, 171–175 (1971).
46. Hartley, T., Trinkler, I. & Burgess, N. Geometric determinants of human spatial memory. *Cognition* **94**, 39–75 (2004).

47. Schuck, N. W., Doeller, C. F., Polk, T. A., Lindenberger, U. & Li, S.-C. Human aging alters the neural computation and representation of space. *NeuroImage* **117**, 141–150 (2015).
48. Taube, J. S., Valerio, S. & Yoder, R. M. Is navigation in virtual reality with fMRI really navigation? *J. Cogn. Neurosci.* **25**, 1008–1019 (2013).
49. Campbell, M. G. et al. Principles governing the integration of landmark and self-motion cues in entorhinal cortical codes for navigation. *Nat. Neurosci.* **21**, 1096–1106 (2018).
50. Chen, G., Lu, Y., King, J. A., Cacucci, F. & Burgess, N. Differential influences of environment and self-motion on place and grid cell firing. *Nat. Commun.* **10**, 630 (2019).
51. Boto, E. et al. Moving magnetoencephalography towards real-world applications with a wearable system. *Nature* **555**, 657–661 (2018).
52. Cadwallader, M. Problems in cognitive distance: implications for cognitive mapping. *Environ. Behav.* **11**, 559–576 (1979).
53. Sadalla, E. K., Burroughs, W. J. & Staplin, L. J. Reference points in spatial cognition. *J. Exp. Psychol.* **6**, 516–528 (1980).
54. Thorndyke, P. W. Distance estimation from cognitive maps. *Cogn. Psychol.* **13**, 526–550 (1981).
55. McNamara, T. P. Mental representations of spatial relations. *Cogn. Psychol.* **18**, 87–121 (1986).
56. McNamara, T. P. & Diwadkar, V. A. Symmetry and asymmetry of human spatial memory. *Cogn. Psychol.* **34**, 160–190 (1997).
57. Newcombe, N., Huttenlocher, J., Sandberg, E., Lie, E. & Johnson, S. What do misestimations and asymmetries in spatial judgement indicate about spatial representation? *J. Exp. Psychol.* **25**, 986–996 (1999).
58. Brunec, I. K., Javadi, A.-H., Zisch, F. E. L. & Spiers, H. J. Contracted time and expanded space: the impact of circumnavigation on judgements of space and time. *Cognition* **166**, 425–432 (2017).
59. Jafarpour, A. & Spiers, H. Familiarity expands space and contracts time. *Hippocampus* **27**, 12–16 (2017).
60. O'Keefe, J. & Nadel, L. *The Hippocampus as a Cognitive Map* (Clarendon Press, 1978).
61. Bellmund, J. L. S., Deuker, L., Navarro Schröder, T. & Doeller, C. F. Grid-cell representations in mental simulation. *eLife* **5**, e17089 (2016).
62. Horner, A. J., Bisby, J. A., Zotow, E., Bush, D. & Burgess, N. Grid-like processing of imagined navigation. *Curr. Biol.* **26**, 842–847 (2016).
63. Byrne, P., Becker, S. & Burgess, N. Remembering the past and imagining the future: a neural model of spatial memory and imagery. *Psychol. Rev.* **114**, 340–375 (2007).
64. Buckner, R. L. The role of the hippocampus in prediction and imagination. *Annu. Rev. Psychol.* **61**, 27–48 (2010).
65. Hasselmo, M. E. *How We Remember: Brain Mechanisms of Episodic Memory* (MIT Press, 2011).
66. Bellmund, J. L. S., Gärdenfors, P., Moser, E. I. & Doeller, C. F. Navigating cognition: spatial codes for human thinking. *Science* **362**, eaat6766 (2018).
67. Constantinescu, A. O., O'Reilly, J. X. & Behrens, T. E. J. Organizing conceptual knowledge in humans with a gridlike code. *Science* **352**, 1464–1468 (2016).
68. Delorme, A. & Makeig, S. EEGLAB: an open source toolbox for analysis of single-trial EEG dynamics including independent component analysis. *J. of Neurosci. Methods* **134**, 9–21 (2004).
69. Lakens, D. Calculating and reporting effect sizes to facilitate cumulative science: a practical primer for *t*-tests and ANOVAs. *Front. Psychol.* **4**, 863 (2013).
70. Hentschke, H. & Stüttgen, M. C. Computation of measures of effect size for neuroscience data sets. *Eur. J. Neurosci.* **34**, 1887–1894 (2011).
71. Berens, P. CircStat: A MATLAB toolbox for circular statistics. *J. Stat. Softw.* **31**, 10 (2009).
72. Cakmak, T. & Hager, H. Cyberith virtualizer: a locomotion device for virtual reality. In *Proc. ACM SIGGRAPH 2014 Emerging Technologies* https://doi.org/10.1145/2614066.2614105 (ACM, 2014).
73. Brainard, D. H. The Psychophysics Toolbox. *Spatial Vision* **10**, 433–436 (1997).
74. Bellmund, J. L. S., Deuker, L. & Doeller, C. F. Mapping sequence structure in the human lateral entorhinal cortex. *eLife* **8**, e45333 (2019).
75. Stemmler, M., Mathis, A. & Herz, A. V. M. Connecting multiple spatial scales to decode the population activity of grid cells. *Sci. Adv.* **1**, e1500816 (2015).
76. Kass, R. E. & Raftery, A. E. Bayes factors. *J. Am. Stat. Assoc.* **90**, 773–795 (1995).

Acknowledgements

We thank J. N. Pereira for pilot work that led to the final experimental design. The research of C.F.D. is supported by the Max Planck Society, the European Research Council (ERC-CoG GEOCOG 724836), the Kavli Foundation, the Centre of Excellence scheme of the Research Council of Norway—Centre for Neural Computation (223262), The Egil and Pauline Braathen and Fred Kavli Centre for Cortical Microcircuits, the National Infrastructure scheme of the Research Council of Norway—NORBRAIN and the Netherlands Organisation for Scientific Research (NWO-Vidi 452-12-009; NWO-Gravitation 024-001-006; NWO-MaGW 406-14-114; NWO-MaGW 406-15-291). C.B. and W.C. are supported by a Wellcome Senior Research Fellowship (212281/Z/18/Z). The funders had no role in study design, data collection and analysis, decision to publish or preparation of the manuscript.

Author contributions

J.L.S.B., C.B. and C.F.D. conceived the experiment. J.L.S.B., T.A.R., M.N. and C.F.D. designed the experiment. T.A.R. collected the data. J.L.S.B. analysed the data and wrote the manuscript with input from M.N., C.B. and C.F.D. W.C. performed the model analysis under supervision of C.B. All of the authors discussed the results and contributed to the final manuscript.

Competing interests

The authors declare no competing interests.

Additional information

Extended data is available for this paper at https://doi.org/10.1038/s41562-019-0767-3.

Supplementary information is available for this paper at https://doi.org/10.1038/s41562-019-0767-3.

Correspondence and requests for materials should be addressed to J.L.S.B. or C.F.D.

Peer review information Primary Handling Editor: Marike Schiffer.

Reprints and permissions information is available at www.nature.com/reprints.

Publisher's note Springer Nature remains neutral with regard to jurisdictional claims in published maps and institutional affiliations.

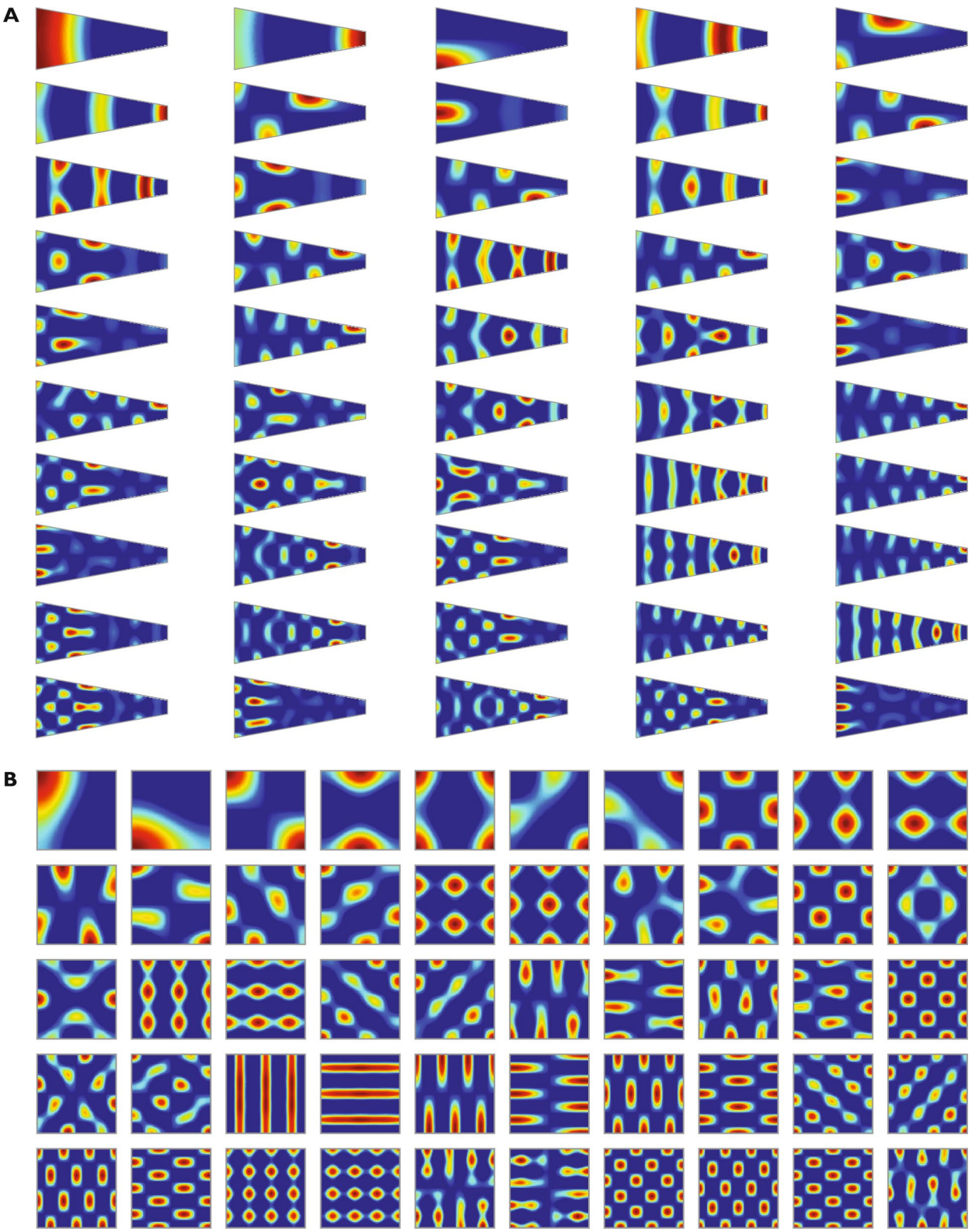

Extended Data Fig. 1 | Successor representation eigenvectors. A,B. The first 50 eigenvectors of the successor representation from a trapezoid and a square environment were used for analysis.

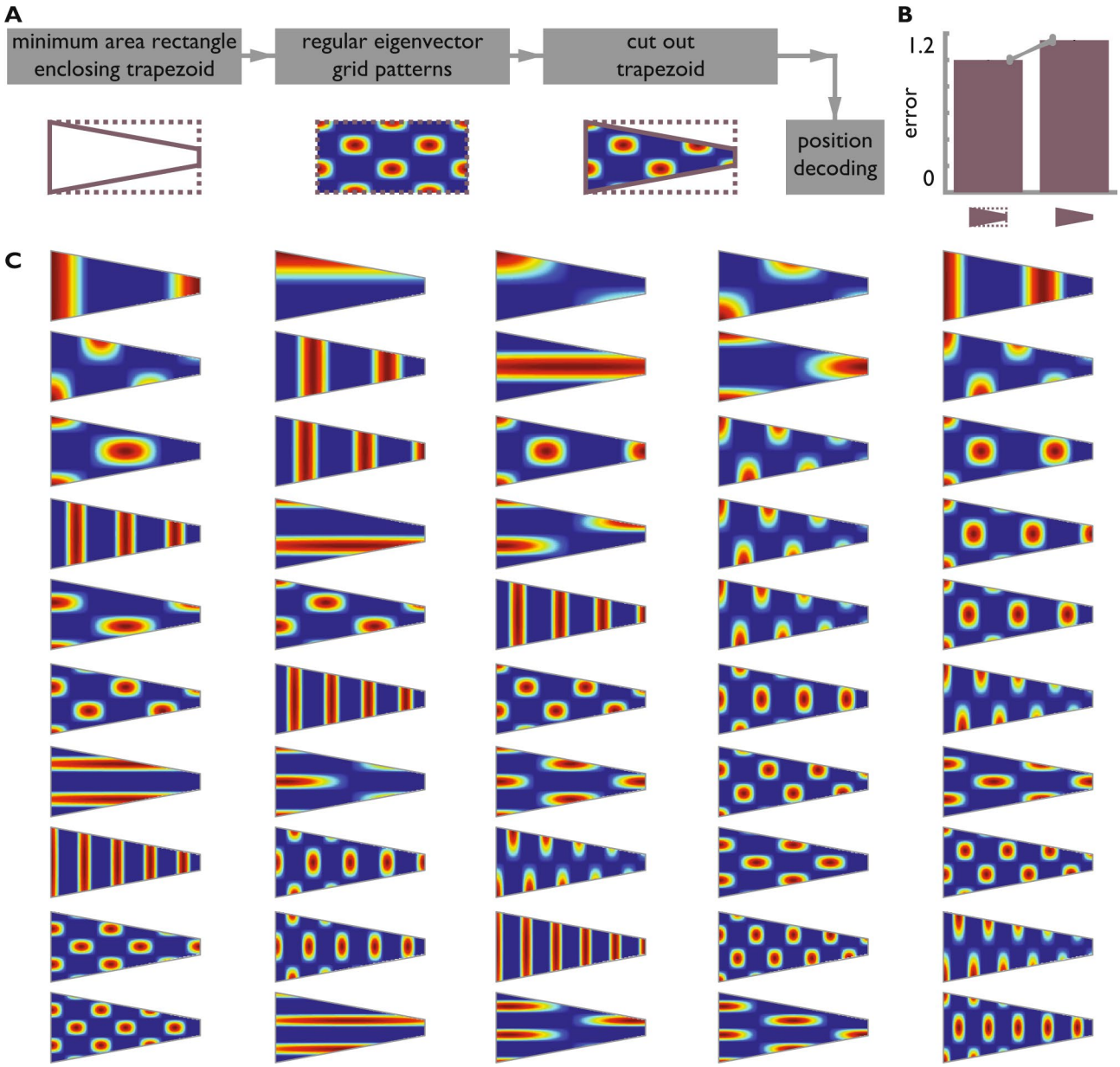

Extended Data Fig. 2 | Position decoding based on the smallest rectangle enclosing the trapezoid. A. To demonstrate that worse position decoding in the trapezoid is due to the distorted eigenvector grid patterns and not the elongated shape of the environment we analyzed the eigenvectors of the smallest rectangle enclosing the trapezoid. We repeated the position decoding on the area of the trapezoid based on the SR grid patterns from the smallest rectangle. **B**. Position decoding errors were larger when the analysis was based on the distorted grid patterns of the trapezoid rather than the regular grid patterns generated on the smallest rectangle enclosing the trapezoid (two-sample t-test: $t(58)=64.52$, $p<0.001$, $d=16.44$, 95%-CI: 14.29; 20.46). **C**. The 50 eigenvector grid patterns used in this analysis.

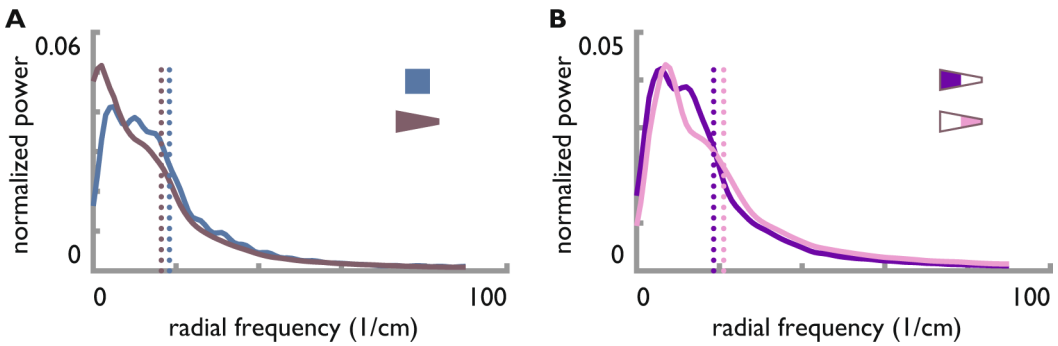

Extended Data Fig. 3 | Spatial frequencies of eigenvector grid patterns. A,B. Radial power spectra based on two-dimensional FFT averaged across the 50 SR grid patterns. Average spatial frequencies were higher in the square than the trapezoid (**A**) and higher in the narrow compared to the broad part of the trapezoid (**B**). Dotted lines indicate mean radial frequencies.

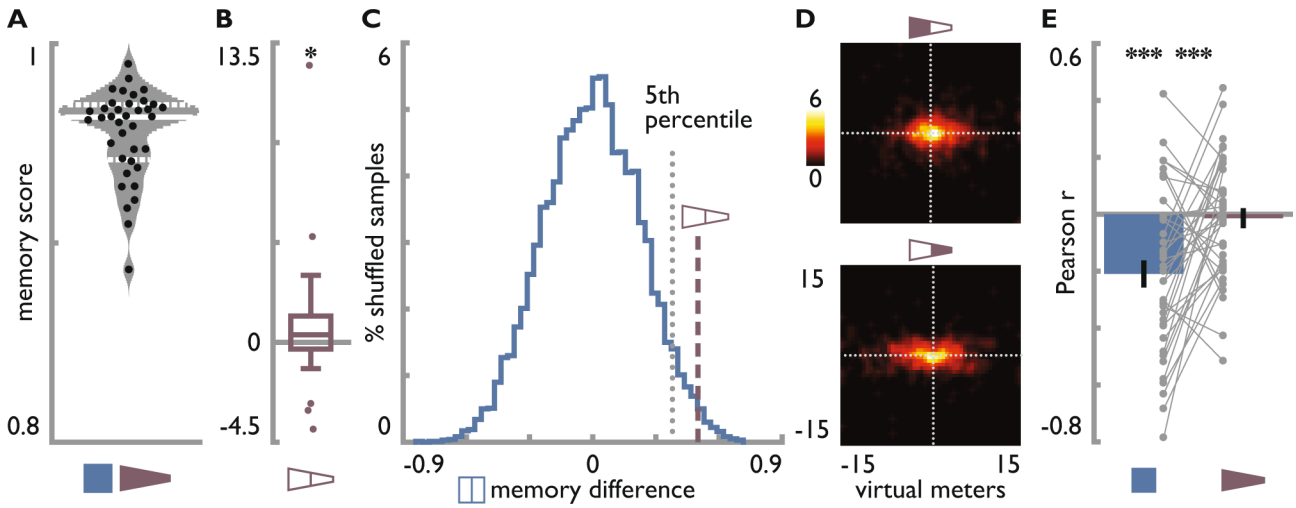

Extended Data Fig. 4 | Positional memory. A. Distribution of average memory scores across participants. Grey area indicates normal kernel density estimate, solid white line shows median and dashed white lines show upper and lower quartile of distribution. Black circles show memory scores of individual participants. **B**. Positional memory error difference between the two parts of the trapezoid. Higher values indicate larger errors in the narrow part of the trapezoid. Data points more than 1.5 times the interquartile range above or below the upper or lower quartile were excluded as outliers (grey dots) for the main analysis, but comparable results are obtained without outlier exclusion ($t(36)=1.50$, $p=0.020$, $d=0.25$, 95%-CI: -0.06; 0.50). Boxplot represents median as well as upper and lower quartile of distribution, whiskers show most extreme value within 1.5 times the interquartile range from the upper and lower quartile respectively. **C**. The positional memory error difference observed between the trapezoid parts (dashed line represents mean difference across participants) was significantly lower than the critical value (5th percentile, dotted line) of a shuffle distribution (blue) obtained from computing error difference between the square halves across 10000 iterations. **D**. Heatmaps showing response locations for all trials across all participants for objects in the broad (top) and narrow (bottom) part of the trapezoid. Dotted lines show correct location in x- and y-dimension with their intersection representing the true position. **E**. Relationships between the distance to the closest boundary and the memory score were quantified using Pearson correlation. Correlation coefficients were consistently negative in the square, indicating better memory for positions closer to the wall. No statistically significant difference from zero was observed for correlation coefficients in the trapezoid and correlations differed between environments. * $p<0.05$ *** $p<0.001$.

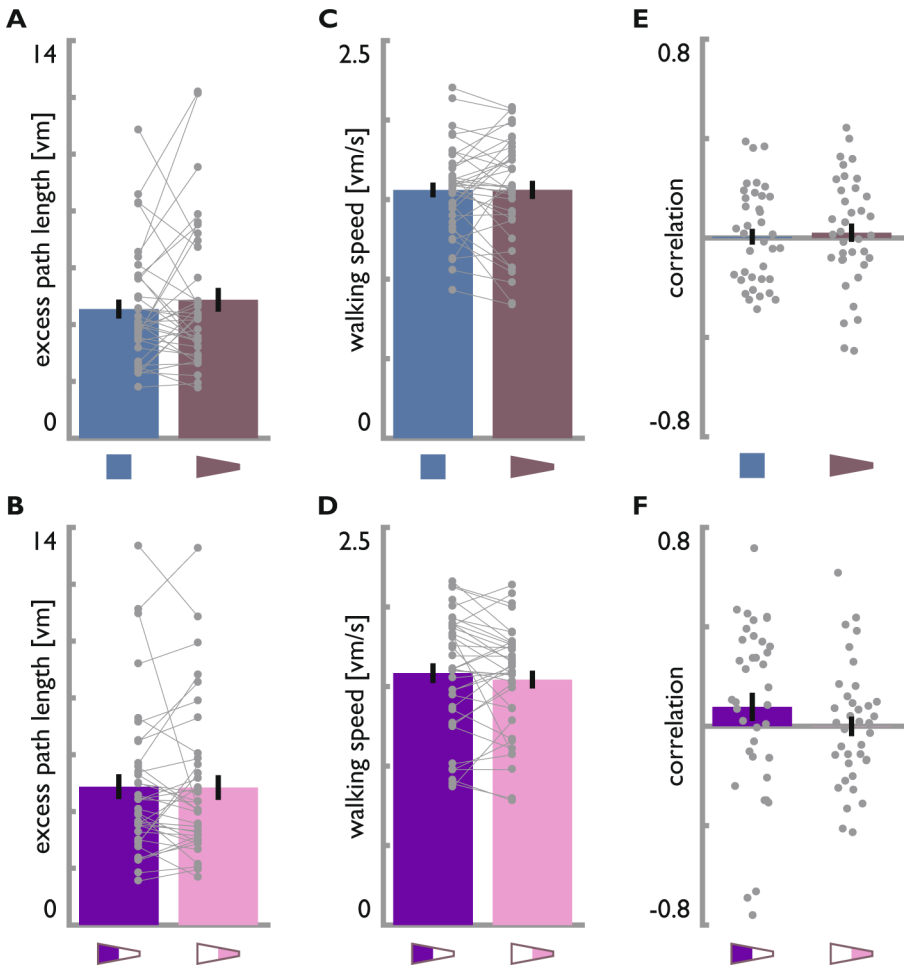

Extended Data Fig. 5 | Navigation performance does not differ between environments. A,**B**. There were no statistically significant differences in the excess path lengths of the trajectories from start to response positions between (**A**) square and trapezoid or (**B**) the two parts of the trapezoid. **C**,**D**. There were no statistically significant differences in walking speed between (**C**) square and trapezoid or (**D**) the two parts of the trapezoid. **E**,**F**. There was no statistically significant difference from zero in Spearman correlation coefficients between the Euclidean distance from the start positions to the correct object positions and replacement errors (**E**) in the square or trapezoid or (**F**) for objects located in the broad and narrow part of the trapezoid separately. Bars show mean±SEM and grey circles indicate individual subject data with lines connecting data points from the same participant.

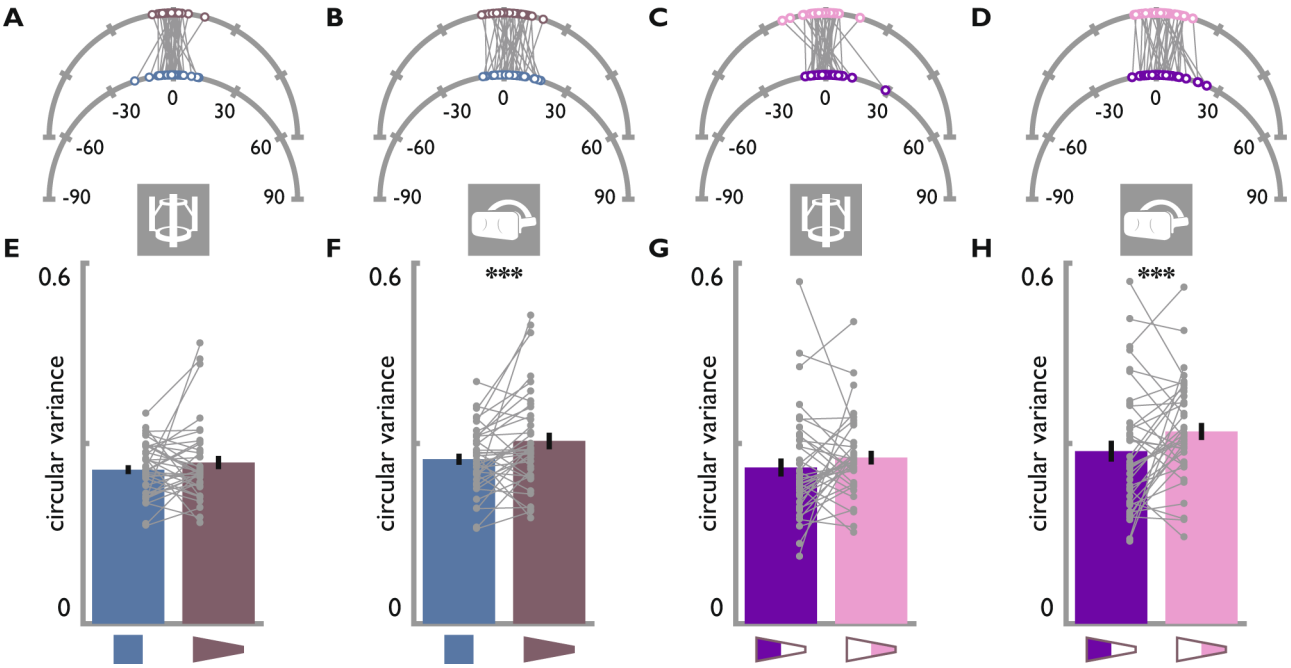

Extended Data Fig. 6 | Head and body orientation during navigation. A,B. Circular means in degrees of (**A**) body and (**B**) head rotations centered on each trial's direction from start to response position. Means were significantly clustered around 0° for both square and trapezoid and there was no statistically significant difference between them. **C,D**. Circular means of (**C**) body and (**D**) head rotations centered on each trial's direction from start to response position. Means were significantly clustered around 0° for trials with target object positions in the broad and narrow part of the trapezoid, respectively, and there was no statistically significant difference between them. **E**. There was no statistically significant difference in the circular variance of body rotations over trials averaged for each participant between square and trapezoid. **F**. The circular variance of head rotations over trials averaged for each participant was larger in the trapezoid than in the square. **G**. There was no statistically significant difference in the circular variance of body rotations over trials averaged for each participant between navigation periods for target objects located in the broad or narrow portion of the trapezoid. **H**. The circular variance of head rotations over trials averaged for each participant was smaller when cued object position were in the broad compared to the narrow part of the trapezoid. *** $p<0.001$.

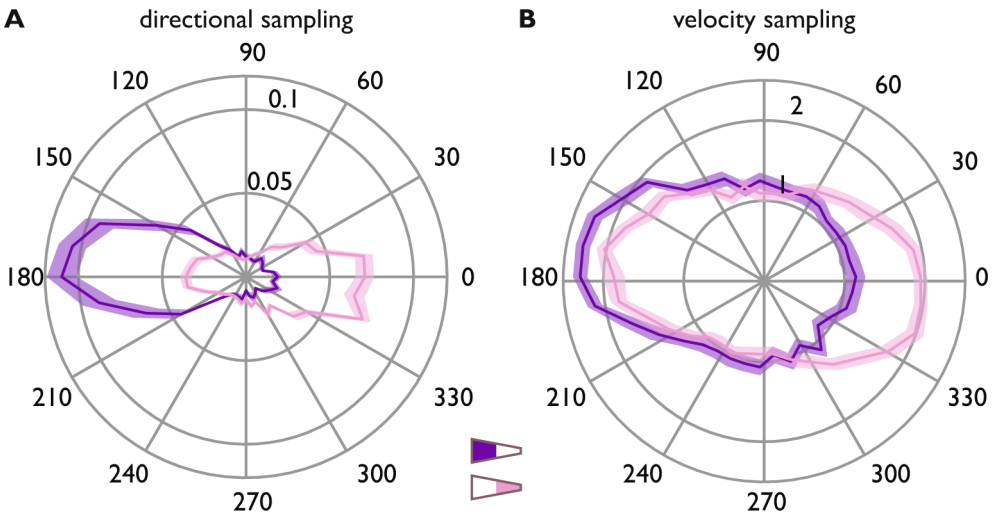

Extended Data Fig. 7 | Angular and velocity sampling. A. Average angular sampling for 10° bins during navigation from a trial's start position to the remembered object location. Radial axis shows proportion of time points facing in a directional bin. For trial's targeting objects in the broad part of the trapezoid, participants mostly faced towards the long base of the trapezoid (180°), whereas they more frequently faced towards the short base (0°) when targeting objects in the narrow part of the environment. **B**. Average movement speed (radial axis vm/s) for 10° directional bins for trials targeting objects in the broad and narrow part of the trapezoid. Navigation speed was higher along the long axis of the environment as indicated by higher movement speeds towards 0° and 180° for trials where participants targeted objects in the narrow and broad part of the trapezoid, respectively. In **A** and **B**, colored lines and shaded area show mean and SEM, respectively.

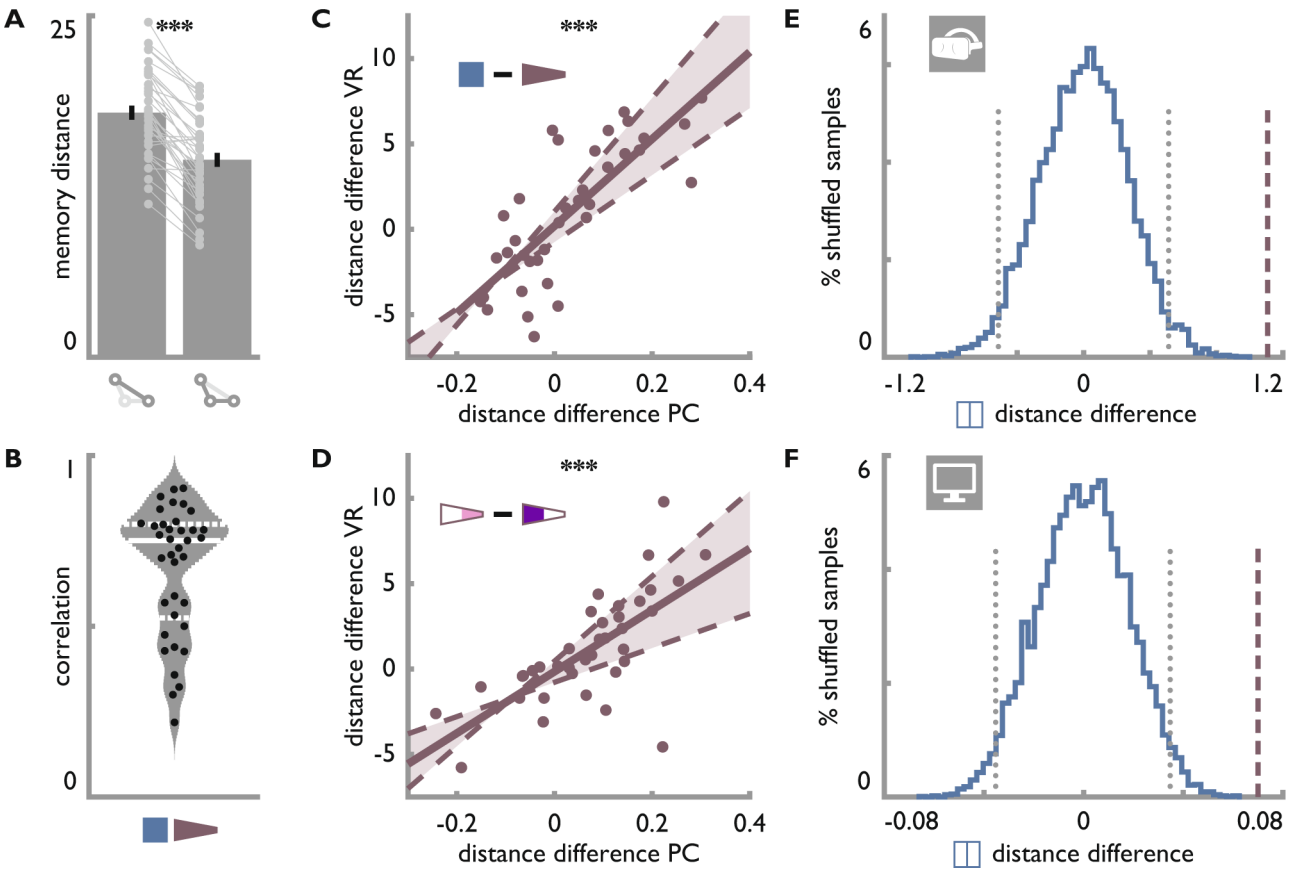

Extended Data Fig. 8 | Distance estimates. A. Long distances (i.e. the base of the isosceles triangle formed by a triplet of positions) were estimated to be longer than the shorter distances (i.e. the legs of the isosceles triangle). Only within-triplet distances were estimated in VR. Bars show mean±SEM and grey circles indicate individual subject data with lines connecting data points from the same participant. **B**. Grey area indicates distribution of Spearman correlation (mean±SD r=0.69±0.19) coefficients between correct and estimated distances based on normal kernel density estimate. Solid white line shows median and dashed white lines show upper and lower quartile. Black circles show correlation coefficients of individual participants. **C**. The difference between distance estimates for identical distances in the square and the trapezoid was highly correlated between the computer screen and the VR version of the task. **D**. Significant correlation of distance difference between the two parts of the trapezoid obtained from distance estimates on the computer screen and in VR. Circles in **C** and **D** denote individual participant data; solid line shows least squares line; dashed lines and shaded region highlight bootstrapped confidence intervals. **E**,**F**. The distance difference observed between the trapezoid parts (dashed line) was more extreme than the critical values (dotted line) of the shuffle distribution (blue) obtained from computing the distance difference between the square halves across 10000 iterations for the distance estimates in VR (**E**) and on the PC (**F**).

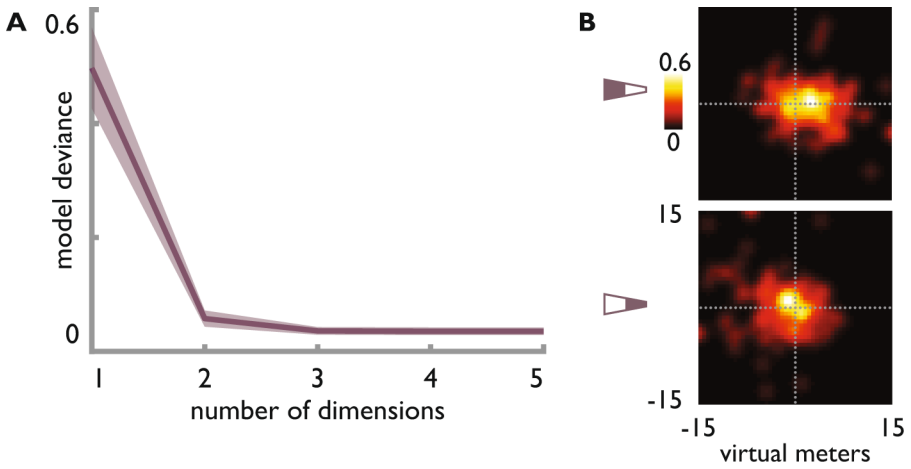

Extended Data Fig. 9 | Two dimensions underlie distance estimates. A. Model deviance of GLMs using pairwise Euclidean distances of coordinates obtained from MDS to predict estimated distances for different numbers of dimensions (solid line shows mean model deviance across participants, shaded area indicates SEM). In line with our a priori assumption that two dimensions underlie the distance estimates, model deviance sharply drops when using two rather than one dimension and there is no substantial benefit from including three or more dimensions. **B**. Heatmaps showing positions reconstructed using multi-dimensional scaling and Procrustes transform for objects in the broad (top) and narrow (bottom) part of the trapezoid. Dotted lines show correct position in x- and y-dimension with their intersection representing the true position.

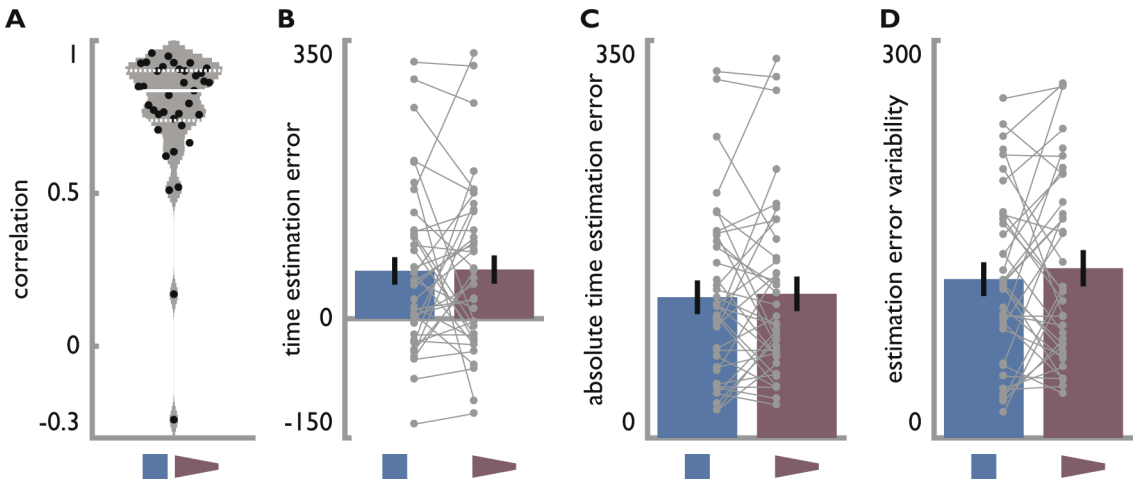

Extended Data Fig. 10 | No statistically significant differences in time estimates between environments. A. Grey area indicates distribution of Spearman correlation coefficients (mean±SD r=0.77±0.23) between true and estimated times based on normal kernel density estimate. Solid white line shows median and dashed white lines show upper and lower quartile. Black circles show correlation coefficients of individual participants. **B-D**. There were no statistically significant differences between the two environments for (**B**) averaged time estimation errors, (**C)** averaged absolute time estimation errors or (**D**) the variability of time estimates as measured by their standard deviation. Bars show mean±SEM and grey circles indicate individual subject data with lines connecting data points from the same participant.

nature research

Corresponding author(s): Jacob L.S. Bellmund, Christian F. Doeller

Last updated by author(s): Oct 28, 2019

Reporting Summary

Nature Research wishes to improve the reproducibility of the work that we publish. This form provides structure for consistency and transparency in reporting. For further information on Nature Research policies, see Authors & Referees and the Editorial Policy Checklist.

Statistics

For all statistical analyses, confirm that the following items are present in the figure legend, table legend, main text, or Methods section.

n/a	Confirmed	
☐	☒	The exact sample size (*n*) for each experimental group/condition, given as a discrete number and unit of measurement
☐	☒	A statement on whether measurements were taken from distinct samples or whether the same sample was measured repeatedly
☐	☒	The statistical test(s) used AND whether they are one- or two-sided *Only common tests should be described solely by name; describe more complex techniques in the Methods section.*
☒	☐	A description of all covariates tested
☐	☒	A description of any assumptions or corrections, such as tests of normality and adjustment for multiple comparisons
☐	☒	A full description of the statistical parameters including central tendency (e.g. means) or other basic estimates (e.g. regression coefficient) AND variation (e.g. standard deviation) or associated estimates of uncertainty (e.g. confidence intervals)
☐	☒	For null hypothesis testing, the test statistic (e.g. *F*, *t*, *r*) with confidence intervals, effect sizes, degrees of freedom and *P* value noted *Give P values as exact values whenever suitable.*
☐	☒	For Bayesian analysis, information on the choice of priors and Markov chain Monte Carlo settings
☒	☐	For hierarchical and complex designs, identification of the appropriate level for tests and full reporting of outcomes
☐	☒	Estimates of effect sizes (e.g. Cohen's *d*, Pearson's *r*), indicating how they were calculated

Our web collection on statistics for biologists contains articles on many of the points above.

Software and code

Policy information about availability of computer code

Data collection	Unreal Engine (v.4.13.2, Epic Games Inc., 2017)Psychophysics Toolbox for Matlab (Release 2016a, The MathWorks, Inc.)
Data analysis	Matlab (Release 2017a, The MathWorks, Inc.) including the Circular Statistics Toolbox (http://www.jstatsoft.org/v31/i10/), EEGLAB and custom code.

For manuscripts utilizing custom algorithms or software that are central to the research but not yet described in published literature, software must be made available to editors/reviewers. We strongly encourage code deposition in a community repository (e.g. GitHub). See the Nature Research guidelines for submitting code & software for further information.

Data

Policy information about availability of data

All manuscripts must include a data availability statement. This statement should provide the following information, where applicable:

- Accession codes, unique identifiers, or web links for publicly available datasets
- A list of figures that have associated raw data
- A description of any restrictions on data availability

The data that supports the findings of this study are available from the corresponding authors upon request.

Field-specific reporting

Please select the one below that is the best fit for your research. If you are not sure, read the appropriate sections before making your selection.

☒ Life sciences ☐ Behavioural & social sciences ☐ Ecological, evolutionary & environmental sciences

Life sciences study design

All studies must disclose on these points even when the disclosure is negative.

Sample size	Sample size was based on a power calculation assuming a small to medium effect (d=0.4) of environmental geometry on human spatial cognition, resulting in a sample size of 52 to achieve a statistical power of 80% (α=0.05, two-tailed test).
Data exclusions	14 incomplete datasets due to technical difficulties with the VR setup or motion sickness.2 participants were excluded due to poor memory performance defined as average replacement errors more than 1.5 times the interquartile range larger than the upper quartile of average errors in the sample.
Replication	One behavioral study was conducted and replication was not attempted.
Randomization	Participants were not grouped and hence no randomization was performed. The order of environments was counter-balanced across participants and object positions were randomized for each participant following the constraints described in the methods section.
Blinding	Participants were not grouped and hence no blinding procedure was performed.

Reporting for specific materials, systems and methods

We require information from authors about some types of materials, experimental systems and methods used in many studies. Here, indicate whether each material, system or method listed is relevant to your study. If you are not sure if a list item applies to your research, read the appropriate section before selecting a response.

Materials & experimental systems

n/a	Involved in the study
☒	☐ Antibodies
☒	☐ Eukaryotic cell lines
☒	☐ Palaeontology
☒	☐ Animals and other organisms
☐	☒ Human research participants
☒	☐ Clinical data

Methods

n/a	Involved in the study
☒	☐ ChIP-seq
☒	☐ Flow cytometry
☒	☐ MRI-based neuroimaging

Human research participants

Policy information about studies involving human research participants

Population characteristics	Healthy young adults (mean age 23.8±2.5 years, 36% female)
Recruitment	Participants were recruited via online platforms and posters on the university campus.
Ethics oversight	Regionale komiteer for medisinsk og helsefaglig forskningsetikk (REK, https://helseforskning.etikkom.no/). For details of the specific project see: https://helseforskning.etikkom.no/prosjekterirek/prosjektregister/prosjekt?p_document_id=809788&p_parent_id=816439

Note that full information on the approval of the study protocol must also be provided in the manuscript.